Materials Science Forum Vol. 590 (2008) pp 29-56
Online available since 2008/Aug/19 at www.scientific.net

doi:10.4028/www.scientific.net/MSF.590.29

Dislocations in Silicon and D-Band Luminescence for Infrared Light Emitters

V. Kveder[1,a] and M. Kittler[2,3,b]

[1]Institute of Solid State Physics, 142432 Chernogolovka, Russia

[2]IHP, Im Technologiepark 25, 15236 Frankfurt (Oder), Germany
[3]IHP/BTU Joint Lab, Konrad-Wachsmann-Allee 1, 03046 Cottbus, Germany

[a]kveder@issp.ac.ru, [b]kittler@ihp-microelectronics.com

Keywords: Dislocations, D-band Luminescence, LED, Silicon

Abstract. There is a growing demand for a silicon-based light emitters generating a light with a wavelength in of 1.3-1.6 μm range, which can be integrated into silicon chips and used for in-chip opto-electronic interconnects. Among other possibilities, the D1 luminescence at about 1.55 μm, caused by dislocations in Si, can be a suitable candidate for such in-chip light emitters. Here we present a brief review of today knowledge about electronic properties of dislocations in silicon and dislocation-related luminescence in connection with possible application of this luminescence for silicon infrared light-emitting diodes (Si-LEDs).

Introduction

It is predicted that optical interconnects will be added in the near future to silicon-based integrated circuits (IC) in order to solve problems caused by the traditional interconnect system [1], such as heat penalty, speed limit, cross-talk etc. For this reason silicon microphotonics, a technology, which merges photonics and microelectronics, is a hot topic for research.

Silica wave-guides are not interesting for integration into silicon IC because of their large dimensions. The most promising are silicon on insulator (SOI) or polysilicon based wave-guides that have a small size due to the large refractive index mismatch and, therefore, allow a large number of optical components to be integrated within a small area. Many key photonic components compatible with Si-CMOS technology and silicon wave-guides have already been demonstrated, as for example, a fast Si based electro-optical modulator [2], and a fast and sensitive Ge detector [3].

All these components can work only with photons with a wavelength in the range of 1.3-1.6 μm, where undoped silicon is transparent. So, there is a strong demand for a silicon-based light emitters, which can be integrated into silicon IC and generate a light with a wavelength in this range. Different approaches for such light emitters have been studied (for review see [1]). Among them are intra-atomic optical transitions in Er atoms in Er-doped Si [4, 5] or Er-doped silicon nano-particles embedded in silicon oxide [6, 7], luminescence of β-$FeSi_2$ precipitates in Si [8, 9] and optical transitions in SiGe superlattices [10] where a relaxation of the k-selection rule can be expected.

Despite the fact that silicon is an indirect band-gap semiconductor, in principal it has the potential to emit the band-to-band line with about 30% efficiency [11] at 300 K. However the silicon band-to-band luminescence has a wavelength of about 1.1 μm and cannot be used with silicon wave-guides. Recently, the D1 luminescence close to 1.55 μm, caused by dislocations in Si, has been demonstrated to be a promising candidate for the on-chip light emitter [12, 13]. The photoluminescence associated with dislocations in silicon was detected for the first time at T = 4.2 K about 30 years ago [14] and in the past investigated quite extensively (see, for example, [15-18]). It consists of four broadened lines (or bands), D1 to D4, with their maxima located at low temperature at 0.81 eV, 0.87 eV, 0.93 eV and 0.99 eV respectively. The research activity in this

field was revived a few years ago when electro-luminescence due to the dislocation-related D1-line has been observed for the first time at room temperature (see [19, 20]). Then it was shown in [12, 13] that by using external impurity gettering and hydrogen passivation to reduce the concentration of non-radiative recombination centers it is possible to increase drastically the external efficiency of silicon light-emitting diodes (LEDs) based on dislocation luminescence. The external efficiency of about 0.1% at room temperature has been already demonstrated for dislocation-based Si-LED emitting 1.55 μm light [12, 13]. Obviously, the efficiency of Si-LEDs based on dislocation-related luminescence can be significantly increased further by using of a proper device design (see, for example [21]) and a proper coupling of LED with a wave-guide.

To introduce dislocations into silicon usually macroscopic plastic deformation is used by applying mechanical stress to the sample at elevated temperature $T_D > 600^oC$. This way of dislocation generation is very convenient for research purposes, but it is, of course, not acceptable for microelectronic technology. However, there are many other methods of reproducible generation of dislocations spatially confined in desirable places that are quite compatible with microelectronic technologies. For example, one can use 'misfit' dislocations or small 'punch-out' dislocation loops, generated around proper impurity precipitates (like Si:Er, β-$FeSi_2$, SiO_2), which can be prepared by ion-implantation and subsequent annealing. Recently a Si wafer direct bonding has been shown to be a convenient way of generation of regular dislocation networks compatible with standard silicon microelectronic technologies [22]. It was already demonstrated that such dislocation networks might be used to build Si-based light emitters for a wavelength of 1.55 μm [23, 24].

Below we present a brief review of what we know now about electronic properties of dislocations in silicon and dislocation-related luminescence in connection with possible application of this luminescence for Si-LEDs. First we briefly discuss the atomic structure of dislocations in silicon, then the electronic properties of dislocations and then the dislocation related luminescence. At the end of the paper we discuss some recent results on luminescence from dislocation networks, prepared by direct bonding of silicon wafers.

Structure of Dislocations in Silicon

Dislocations are line defects in a regular crystal lattice. They keep the lattice translation symmetry along their line direction and may be regarded as a kind of one-dimensional nanostructures. In semiconductors the most interesting and important effect of dislocations results from electronic states, which dislocations introduce into the band gap of semiconductors. Associated to the ideal (straight and clean) dislocation, one should expect one-dimensional electronic energy bands (1D-bands). So the dislocations can be considered as native 'quantum wires'.

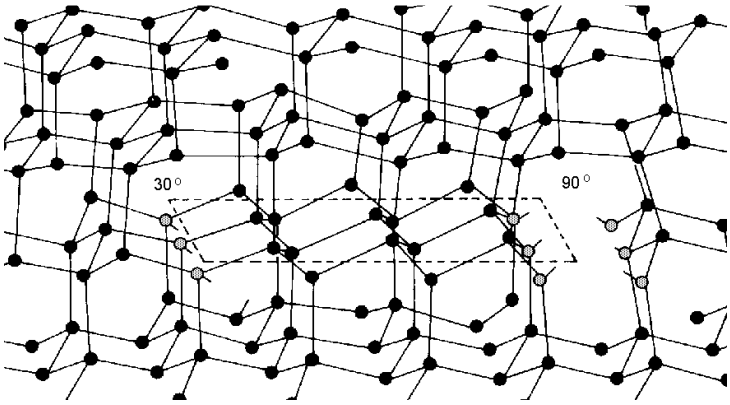

Fig. 1. Structure of a glide set 60^0-dislocation, dissociated into a 30^0-partial (left) and a 90^0-partial Shockley dislocation (right), shown in the unreconstructed state.
According to TEM data, the equilibrium distance d_0 between the two partials in 60^o dislocations is about 5 nm.

For topological reasons, atoms at dislocation core are expected to have a line of dangling bonds, producing 1D-bands with their edges located *deep* in the band gap of semiconductor. However, for some types of dislocations, an atomic reconstruction inside the core is possible, which means that dangling bonds at neighbouring atoms form covalent bonds with each other. In this case the dislocation can usually produce only relatively shallow 1D-bands split off from the conduction band and valence band by strong lattice deformation (strain field) around dislocation. So, the position and properties of 1D-bands, produced by dislocation, must depend strongly on the dislocation type and core geometry.

In the Si crystal the glide planes for moving dislocations are {111}. Their Burgers vectors are of the type <110>. However, there are two possible {111} sets of glide systems for dislocations: the shuffle set when dislocation core is between the widely spaced {111}-planes and the glide set when the core is lying between the narrowly spaced {111}-planes. The dislocations of these two sets have different core structures and must have different electronic properties.

Dislocations of the glide set can dissociate into two parallel Shockley partial dislocations with a stacking fault ribbon between them (see Fig. 1). The geometry of the dangling bonds in their cores allows to decrease strongly the core energy by forming new covalent bonds between the dangling bonds (bond reconstruction) with only small increase of elastic energy.

Dislocation of the shuffle set cannot dissociate into partials, and the dangling bonds of the core are nearly normal to the glide plane. In this case the bond reconstruction needs so large atomic displacement that it seems to be energetically unfavourable.

At present it is widely accepted that in silicon most of dislocations generated at a temperature more than 700^oC by either macroscopic or microscopic plastic deformation are dissociated screws and 60^o dislocations of the glide set (see [25] for review). A perfect 60^0-dislocation of the glide set dissociates into a 90^0- and a 30^0-partial (see Fig. 1), a screw dislocation into two 30^0-partials. According to theoretical calculations the reconstructed partials are energetically favourable.

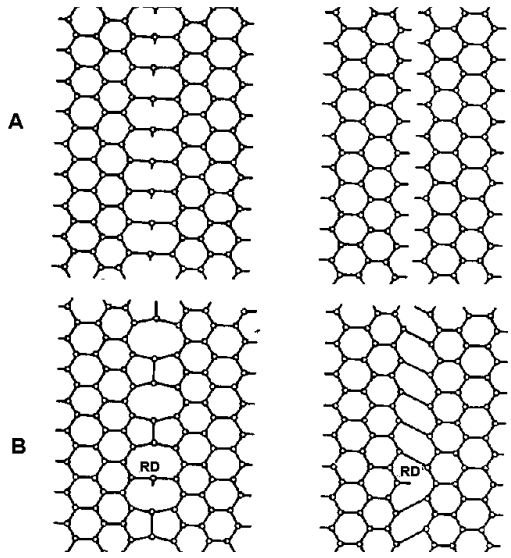

Fig. 2. Core view in the glide (111) plane of 30° (left) and 90° (right) Shockley partial dislocations in their unreconstructed (A) and reconstructed (B) states.

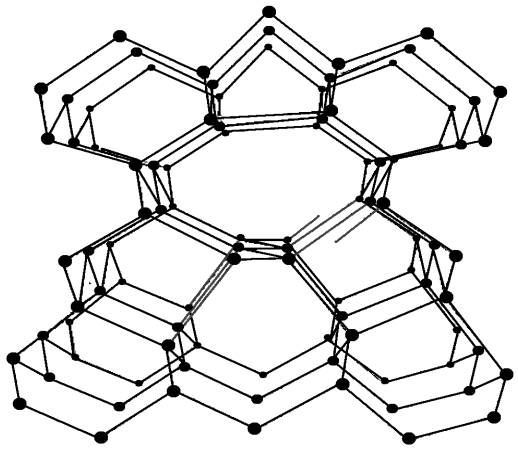

Fig. 3. Possible core structure of a reconstructed Lomer dislocation.

Fig. 2 illustrates how the cores of 90^0- and a 30^0-partial can be reconstructed. The RD is a defect of reconstruction, which contains a dangling bond. At elevated temperature the reconstruction defects can move along dislocation and can disappear when meet each other. So, the concentration of dangling bonds related to reconstruction defects should depend on a thermal prehistory of a sample and it should be possible to reduce their concentration by a proper thermal annealing.

All available experimental data support the theoretical predictions that reconstruction of partial dislocations in Si is energetically favourable. For example, the measurements of electron paramagnetic resonance (EPR) show that concentration of paramagnetic dangling bonds, which can be sometimes quite significant for dislocations introduced at $T < 700\ ^oC$, vanishes after annealing at $T > 850\ ^oC$ [26-28].

One should note that when moving dislocations meet each other they could react producing more complicated constructions. For example, when two 60 °C glide set dislocations with the same line direction in [110] moving in two different glide planes meet each other they can form a new, Lomer type of dislocation (see Fig. 3), which is not mobile and have a core structure and electronic properties very much different from 60° and screw dislocations. Sometimes, when a local density of dislocations is as high as 10^8-10^9 cm^2, the density of Lomer dislocations according to TEM data can be very significant, more than to 10% of total dislocation density, so that their contribution to electronic properties of the sample might become important. Unfortunately, the electronic properties of Lomer dislocations or other complicated constructions that might appear due to dislocation reactions are not well investigated.

Electronic Properties of Dislocations in Silicon

When considering the capture of free electrons and holes and the occupation statistics of electronic energy states at dislocation, we should first of all remember that the capture of free electrons (or holes) to the dislocation creates a Coulomb band-bending $e\Phi$ around the dislocation (see Fig. 4). This electrostatic potential slows down further capturing of free electrons to the dislocation approximately by the factor $exp(-e\Phi/k_BT)$ and finally limits the total equilibrium occupation of dislocation states.

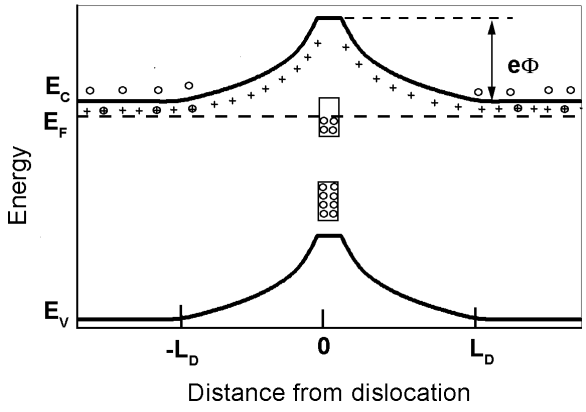

Fig. 4. Illustration of the Coulomb barrier appearing around a dislocation due to its line charge caused by electrons captured to the acceptor dislocation states.

The exact calculation of eΦ is a difficult problem (for details see [25]), but in many cases it can be approximated by simple formula:

$$e\Phi \approx e^2 N_{tot} \cdot \{[ln(N_{tot}(N_{tot}/\pi n_d)^{1/2}]-0.5\}/\varepsilon \quad (1)$$

where N_{tot} is total dislocation charge per unit length (a concentration of electrons or holes captured to all dislocation energy states), ε is the dielectric permittivity of Si and n_d is a concentration of shallow donors (or acceptors) in a sample. Equation 1 assumes that the screening radius L_{scr} of the electric field around the dislocation is:

$$L_{scr} = (N_{tot}/\pi n_d)^{1/2} \quad (2).$$

As a result, the total density N_{tot} of electrons (or holes) captured to the dislocation per unit length usually cannot exceed $N_{tot} = (2\text{-}5)\cdot 10^6$ cm^{-1} even if the total number of states N_{DD} per unit length at the dislocation is much larger than this value.

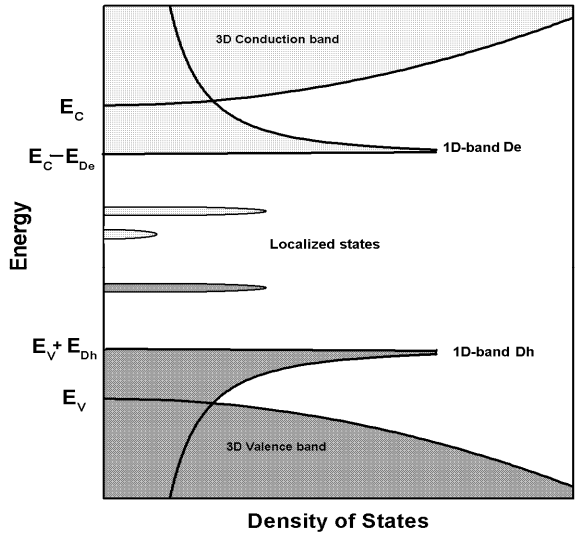

Fig. 5 Energy diagram for a glide 60° dislocation in Si. Regular segments of the dislocation produce 1D-bands, while some defects and irregularities at the dislocation can produce deep localized states.

As it was already mentioned, most of dislocations in Si generated at T > 700°C are screw and 60° dislocations of the glide set, which are dissociated into partial Shockley dislocations with reconstructed cores. Theory predicts that ideal straight and clean segments of such dislocation are not associated with any deep electronic states in the band gap of silicon. However, 60° dislocations must have relatively shallow one-dimensional electronic energy bands (*1D-bands*) caused by the lattice deformation (elastic strain field): the empty one splits down from the conduction band with its bottom at E_C-E_{De}, and the occupied one splits up from the valence band with its top at E_V+E_{Dh} (see Fig. 5). Please, remember that the density of states in 1D electron band has a minimum at the centre and 1/√E-singularities at the band edges, that is much different from the 3D-band where it is zero at band edges, increasing as √E (see Fig. 5).

In addition to the 1D-bands, De and Dh, real dislocations can also have deep localized (0-D) electronic states (see Fig. 5), originating from some „native“ core defects (like reconstruction defects and jogs), from core defects caused by vacancies or impurity atoms incorporated into dislocation core and from impurity atoms bound to dislocation by its strain field in the form of very narrow clouds. Please note, that the electronic energy levels of impurities incorporated into dislocation cores may differ significantly from the energy levels of the same impurities accommodated as individual atoms within the bulk.

On the other hand core defects exert also a significant impact on the 1D-bands. With increasing core defect concentration the wave function in 1D-bands, extending along the dislocation line, becomes more and more localized smoothing the 1/√E singularities in density of states at the energy edges of 1D-bands.

Experimental observation of localized states. In contrast to the one-dimensional bands De and Dh, that are inherent to dislocations, the concentration of deep 0-D electronic states, related to core defects and impurities, depends strongly on sample history and can vary in a very wide range. It may be controlled to a certain extent by anneal treatments. It is known that annealing at $T \geq 800\ ^0C$ leads to a strong reduction of some of core defects, which have been introduced by plastic deformation at lower temperatures. Apparently local equilibriums of intrinsic dislocation core defects are in some way re-established at those temperatures, although dislocations as non-equilibrium defects survive. As soon as the dislocations are forced to move, the point defect equilibriums are again disturbed [25].

To investigate the localized deep states at dislocations deep level transient spectroscopy (DLTS) is widely used. Through the registration of the capacitance transients of a Schottky contact, C(t), it probes the emission kinetics of defects inside the depletion region under the Schottky contact. Since the initial occupation of defects by electrons (or holes) is adjustable by variation of the capture period t_p preceding the emission period t_e, the capture process of the defect can be also investigated by DLTS.

DLTS allows distinguish the defects located at dislocations from point defects in a bulk by measuring dependence of DLTS spectra on capture time duration t_p [29, 30, 31]. In the simplest case, when the concentration of deep defects at dislocation is not very high, so that overlapping of electrons wave functions is small enough to neglect electron hopping, the kinetic equation for the number of electrons N_i^* captured to the dislocation acceptor defects with energy E_i is the following:

$$dN_i^*/dt = (N_i - N_i^*)n\sigma v_{th}\, exp(-e\Phi/k_BT) - N_i^*\sigma v_{th}N_C \cdot exp(-(E_C-E_i)/k_BT) \qquad (3).$$

Here N_i is a concentration of acceptor defects with given energy E_i, σ is a capture cross-section, v_{th} and n are a thermal velocity and concentration of free electrons, N_C is effective density of states in a conduction band. The common capture barrier $e\Phi$ given by Eq.1 with $N_{tot} = \Sigma(N_i^*)$ results in logarithmic dependence of N_i^* on capture time t_p: $N_i^* \sim k_BT\, log(t_p/t_e)$, while for point defects this dependence is exponential. So, observation of logarithmic dependence of DLTS line amplitude on t_p indicates that this DLTS line corresponds to states localized at dislocation (or other extended defect). The behaviour of the DLTS signal with variation of t_p also allows detecting of electron hopping between defects at dislocation [29, 30, 32].

Deep dislocation related energy levels have been intensively investigated by DLTS (see, for example [31-36]) during a quarter of century and we know already quite a lot about their properties. However, the exact origin of the core defects responsible for all these well known dislocation-related deep energy levels detected by DLTS is not yet completely clear.

As an example, Fig. 6 shows a typical DLTS spectrum of deep dislocation-related acceptor states detected in n-Si deformed at 750°C to a dislocation density N_D of about $3 \cdot 10^8\ cm^{-2}$. The DLTS spectrum in the as-deformed sample mainly consists of several overlapping strongly non-uniformly broadened lines B (E_C - 0.3 eV), C (E_C - 0.37-0.43 eV) and D (E_C - 0.54eV), well known in literature [25, 44, 31]. All these lines are always observed for dislocations introduced at T<800°C. They show all characteristic features of deep localized states at extended defects [29-33], like the logarithmic dependence of the signal amplitude on t_p. The total concentration N_{DD} of the B, C, D states, estimated from numerical fitting using an approach [30, 37], is about $(2\text{-}3)\times 10^6\ cm^{-1}$ for the spectrum shown in Fig. 6, but it can be even higher for samples deformed at lower temperature. Line broadening is typical for dislocation-related deep defects and can be usually in the order of 10-50 meV.

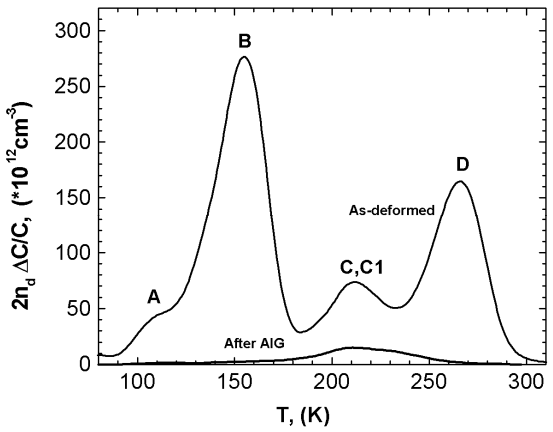

Fig. 6. DLTS spectra of n-FZ-Si ($n_d = n = 2 \cdot 10^{15}$ cm^{-3}) measured in the as-deformed state (curve 1), deformation at 750 °C along [123] (one glide plane) yielding a dislocation density $N_D \approx 3 \cdot 10^8$ cm^{-2}, and after ALG (850°C, 30 min). DLTS: F = 29Hz (t_e = 34ms), $U_b = U_p$ =5V, t_p =0.1ms.

It is known, that the defects B and D are thermally unstable and their concentration can be strongly reduced by annealing at 850-900°C. So, these two lines may correspond to some meta-stable intrinsic core defects. In particular, the D-line is probably related to dangling bonds at dislocations always observed in such samples by the EPR technique. The defects corresponding to the C-line remain nearly unaffected by usual thermal annealing but can be drastically reduced by aluminium gettering (AlG) [38] and hence are probably related to some impurities at dislocations [38, 39]. As on can see in Fig. 6, indeed, AlG at 850°C results in a very strong reduction of not only of B, D lines, but also of a C line.

The concentration of electrically active deep 0-D states at dislocation can be further reduced by hydrogen passivation in a hydrogen plasma at T ≈ 200-350 °C [40-44]. Hydrogen reacts with those defects making them electrically inactive. However, this process is in some way reversible: annealing at T > 700°C may result in releasing of hydrogen and in recovery of electrical activity of the defects. At the same time, hydrogen do not influence dislocation 1D-bands. One cannot exclude that not only the hydrogen, but also some other impurities can passivate electrically active core defects by chemical reactions with them.

As it was already mentioned, a concentration of core defects N_{DD} per unit dislocation length depends on condition of plastic deformation, for example, on the dislocation velocity during dislocation motion. In [32] the dependence of DLTS on the velocity of dislocations and on the distance that dislocations travelled during deformation at 600°C were measured in samples with small (about 10^4-10^5 cm^{-2}) number of long individual dislocations when dislocation reactions or generations of new dislocations were avoided.

Curve 1 in Fig. 7 shows the DLTS spectrum measured for 10^4 freshly prepared dislocation loops with diameter $2D_{path}$ of 510 μm. One can see, that the DLTS signal is nearly absent. Then the same dislocations were forced to move with a very small velocity (less or about 3 μm/min) by applying a stress of 30 MPa at 600 °C and the DLTS were measured depending on the deformation time and a distance D_{path} that dislocation travelled after sequential deformation steps (Fig. 7).

It was found that the concentration of deep acceptor defects, related mainly to the C-line, increases monotonically with the increase of the deformation time and dislocation travel distance. The amplitude of the observed DLTS signal is proportional to the logarithm of refilling pulse duration t_p, that is typical for defects at dislocations.

To prove that the observed DLTS corresponds to defects at dislocations, but not in their trails, a stress of about 90MPa was applied at 600°C to this sample that forced the dislocations to move a distance of 100 μm with a high velocity of 10 μm/min. The trailing path of each dislocation increased only by 10% compared with one for spectrum 4. However, instead of increasing, the DLTS spectrum decreased drastically (see curve 5 in Fig. 7).

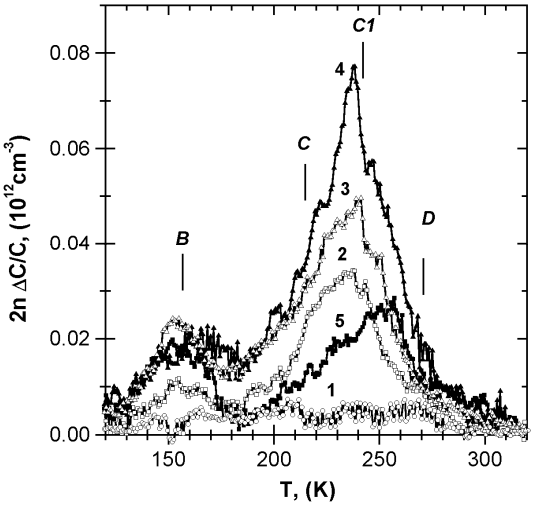

Fig. 7. DLTS spectra in sample N-21, depending on the distance D_{path} that dislocation travelled with a velocity of 3 μm/min at 600 °C during sequential deformation steps: (1) D_{path} = 0 μm, (2) D_{path} = 295 μm, (3) D_{path} = 615 μm, (4) D_{path} = 1060 μm. Spectrum (5) was measured after additional travel of the same dislocations to a distance of 100 μm with a velocity of 3 μm/min. DLTS parameters are: U_b = 5V, U_p = 4V, t_p = 0.1ms, t_e = 34ms (F = 28.6 Hz) [32].

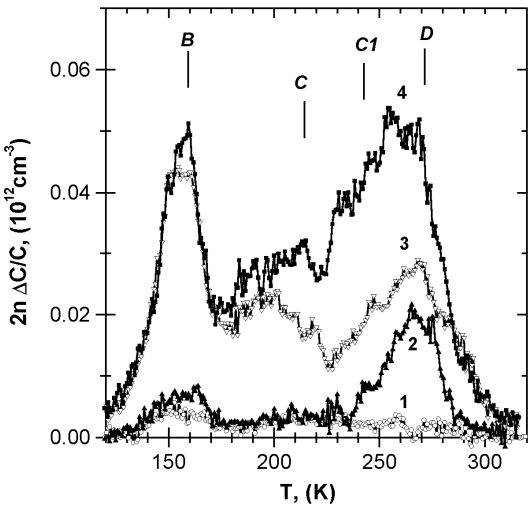

Fig. 8. DLTS spectra in sample N-20, depending on the distance D_{path} that the dislocations travelled with a velocity of 5-6 μm/min at 600°C: (1) D_{path} = 0 μm, (2) D_{path} = 130 μm, (3) D_{path} = 435 μm, (4) D_{path} = 675 μm. DLTS parameters are: U_b = 5V, U_p = 4V, t_p = 0.1 ms, t_e = 34 ms (F = 28.6 Hz) [32].

The most probable explanation of this result is the following: When dislocations are moving slowly, they collect impurities responsible for C, C1 centers, and the DLTS signal increases. However, if we force dislocations to move with a high velocity, the impurity atoms cannot follow dislocations anymore so that the dislocations loose nearly all impurity atoms accumulated before.

So, the high-speed dislocation motion can clean dislocations from impurities. However, in addition to collection impurities, some intrinsic core defects can be generated during dislocation motion. Fig. 8 (see [32]) shows the dependence of DLTS spectra on dislocations travelling distance when they moved at 600°C with a velocity of 5-6 μm/min under the stress of 60 MPa. One can see that the amplitude of C lines is now significantly smaller than in sample N-21 (see Fig. 7) for the same travel distance, but concentration of defects responsible for so-called D-line is higher.

Experimental observation of 1D-bands. Let us discuss now the experimental evidences for 1D-bands. How one can distinguish experimentally the 1D-bands with rather large localization length L of wave functions along dislocation from dislocation 0-D electronic energy states of core defects with strongly localized wave functions?

1D-bands usually cannot be detected by DLTS, except for some special cases [44]. Indeed, the thickness L_{SC} of depletion region under the Schottky contact, where the DLTS probes the thermal emission of electrons, is usually small (a few microns) and the electric field U_b/L_{SC} in this region is very high (> 10^4 V/cm). So, for dislocation crossing the depletion region, the electrons captured to 1D-band will quickly leave the depletion region just by drift in 1D-band along dislocation without being thermally activated to the 3D-conduction band.

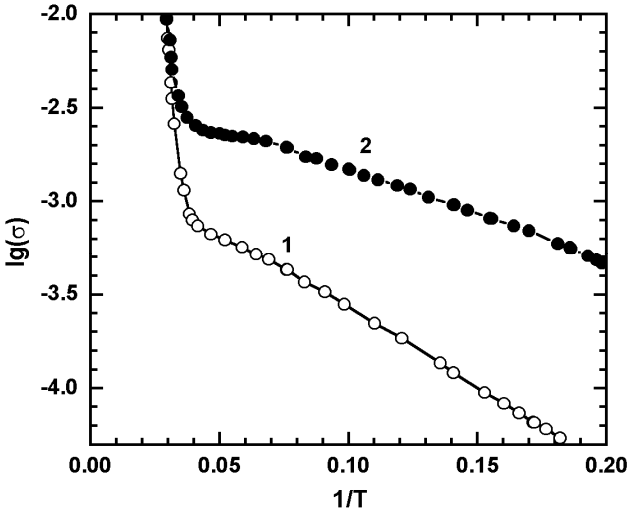

Fig. 9. Typical temperature dependence of the conductance σ measured at 9300 MHz in a p-Si sample with dislocations introduced at 850 °C.
(1) As-deformed sample, (2) the same sample after additional high stress deformation at 450 °C to make the dislocations more straight. The conduction below 20 K is caused by the motion of holes in 1-D bands, while the sharp increase at T > 20 K is due to thermal activation of free holes to the 3-D valence band from shallow boron acceptors.

The first experimental evidence of the 1D-band existence came from the measurements of microwave absorption (see Fig. 9) caused by motion of electrons and holes captured to 1D-bands E_{De} and E_{Dh} [45-49].

Even more convincing and comprehensive data about dislocation 1D-bands associated with 60° and with Lomer dislocations were obtained from the measurements of so-called "electric-dipole spin resonance" (EDSR) [50-56]. The EDSR is based on the fact that due to spin-orbit interaction in a system without inversion symmetry the term V[pS] appears in electron Hamiltonian [57, 58]. This term couples the electron spin S with its momentum p. It means that the modulation of the electron momentum p by the microwave electric field E_ω with a frequency ω can excite the transition between the Zeeman spin levels of electron. Therefore the resonance singularity, called EDSR, must appear in a sample dielectric permittivity $\varepsilon = \varepsilon' + i\varepsilon''$ measured at frequency ω in a static magnetic field $H_0 = \hbar\omega/g\mu_B$, corresponding to spin resonance.

Due to high symmetry of the silicon crystal the coefficient V is zero for free electrons and holes and the EDSR signal is absent for them. However, the local symmetry of dislocation core is lower than of Si-crystal and has no inversion symmetry. Therefore, the value of V can be very large for electrons in dislocation electronic states. At the same time, for localized states at core defects the EDSR is again nearly zero since the modulation of momentum p by microwave field E_ω is nearly zero in this case. And only for electrons or holes in 1D-bands the EDSR will be really large, much more than the usual EPR signal when the E_ω is applied parallel to dislocation line. In this case the EDSR signal Δε is proportional to:

$$\Delta\varepsilon \sim n_{1D}[V\mu_\omega \cdot S(L_{loc}/L_D)\cos(\alpha))^2(\hbar\,\Omega^2/(k_BT(\omega-\Omega+i/\tau_2)] \qquad (4)$$

where L_{loc} is the length of electron localization in 1D-band along the dislocation, n_{1D} is the density of electrons in 1D-band at dislocation, $\mu_\omega = e\tau/m^*(1+i\omega\tau)$ is the electron mobility in 1D-band, α is the angle between electric field E_ω and the dislocation line, $\Omega = g\mu_B H_0/\hbar$ is the spin resonance frequency and τ_2 is the spin relaxation time. The function $S(x)$ is

$$S(x) = 1 - \exp(i\pi/4)\,th(x \cdot \exp(-i\pi/4)/x \qquad (5)$$

The parameter L_D is:

$$L_D = \{e \cdot \mu_\omega \cdot n_{1D}[\log(L_{loc}^2/r^2)]/\varepsilon\omega\}^{1/2} \qquad (6)$$

where r is the radius of the wave function of electrons in 1D-band in directions perpendicular to dislocation, that is expected to be not larger than a 1-2 nm. Since the function *S(x)* is complex, the shape of experimentally measured absorption Im(Δε) or dispersion Re(Δε) EDSR signal is always a mixture of absorption and dispersion Lorentzian curves. So, not only the amplitude, but also the shape of EDSR resonance line depend strongly on the parameter L_{loc}/L_D. Simultaneous analysis of shape, amplitude and anisotropy of EDSR line allows determining localisation length L_{loc}, mobility μ_ω and g-value of electrons (or holes) in 1D-band for dislocation with different line directions.

Using this technique the existence of 1D-bands was proven for 60° dislocations and for Lomer dislocations in Si. It was shown that for specially prepared [59] straight dislocations the L_{loc} along dislocation exceeds 300-500 nm even at T < 5 K [54, 56] and that it can vary strongly [53,54] depending on dislocation prehistory determinative for core defects concentration.

To estimate the energy positions E_{De} and E_{Dh} of the edges of 1D-bands (see Fig. 5), the photo-excitation spectrum of the EDSR signal, corresponding to holes in 1D-band E_{Dh}, was measured [54] for straight 60° dislocations in Si. The result is shown in Fig. 10. The dependence of the EDSR intensity ΔA on the light energy shows distinct thresholds at the band gap energy of Si $E_G \approx 1.17$ eV and also at $E_1 \approx 1.08$ eV (E_G-$E_1 \approx 0.09$ eV) and $E_2 \approx 1.0$ eV (E_G-$E_2 \approx 0.17$ eV).

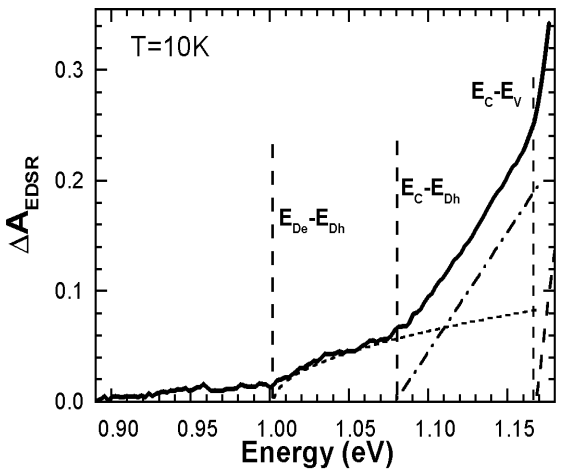

Fig. 10. Change of the amplitude of the EDSR signal for holes in the 1D-band E_{Dh} caused by photo-excitation depending on the photon energy [54].

It was adopted in [54] that the threshold at E_2 corresponds to optical excitation of no-phonon electronic transitions from 1D-band E_{Dh} to the 1D-band E_{De} (see Fig. 5), while the threshold at the energy E_1 corresponds to the transitions from 1D-band E_{Dh} to the conduction band E_C. Thus, the energy depths of the edges of 1D-bands are nearly the same for both 1D-bands, namely, (E_C-E_{De}) ≈ (E_{Dh}-E_V) ≈ 80-85 meV. These values for (E_C-E_{De}) and (E_{Dh}-E_V) are quite close to the values (E_{Dh}-E_V) ≈ 65 meV and (E_C-E_{De}) ≈ 85 meV calculated in [40] from temperature dependences of conductivity in specially prepared p- and n- samples where the deep core defects were strongly passivated by hydrogen. Similar results, (E_{Dh}-E_V) ≈ 70 meV and (E_C-E_{De}) ≈ 80 meV have been also obtained in [60] from measurements of temperature dependence of microwave conductivity in plastically deformed n- and p-type Si crystals.

Transport of charge carriers along dislocation networks. Individual dislocation is a 1D system and the length of electronic transport along it is limited by the presence of defects and potential fluctuations at dislocation line. However in case of dense dislocation network that can be, for example, prepared by Si wafer direct bonding, the electronic tunneling between dislocations becomes possible. It makes the system quasi-2-dimensional and electronic transport in large distance becomes possible. That was demonstrated in [61, 62] by EBIC measurements and also by direct measurements of DC conduction [63]. A dislocation network was formed within a 40 nm thick SOI layer with p-type conductivity and Ohmic contacts were fabricated at a distance of 1 μm, see Fig. 11. The I-V characteristics measured at 300 K is shown in Fig. 11. The measured resistance of the structure is of about $R_{disl} \approx 4x10^2$ Ω, while for the similar reference structure, *without* a dislocation network in a 40 nm thick SOI layer, a resistance is much higher, of about $R_{ref} \approx 2x10^6$ Ω.

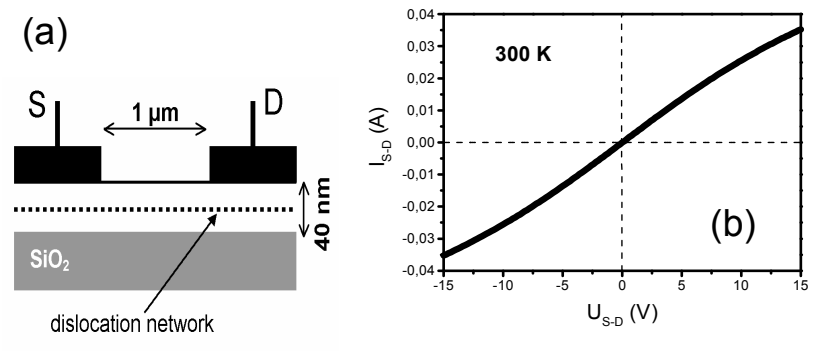

Fig. 11. (a) Schematic view of the sample containing a dislocation network within a 40 nm thick SOI layer of p-type. The Ohmic contacts (S and D) are 5 μm wide and located at a distance of 1 μm.
(b) I-V characteristics at 300 K revealing Ohmic character, yielding R_{disl} = 4x10^2 Ω. With decrease of temperature the resistance R_{disl} was reducing. In the reference sample without dislocations R_{ref} = 2x10^6 Ω was observed. For details see also [63].

Recently, a significant reduction of R caused by a dislocation network in a p-type SOI layer was also reported in [64]. So, the highly conductive dislocations networks can be considered as a very promising system for new type of FETs with a very high frequency performance.

Electron-hole recombination at dislocations.

The D-band luminescence is a result of radiative electron-hole recombination via dislocation-related electronic states. The efficiency of luminescence is determined by competition of radiative and non-radiative recombination and only a clear comprehension of recombination processes at dislocations can give a chance to find a way for increasing this efficiency. The knowledge about recombination at dislocations in silicon is also of a great importance for quickly developing solar cell industry based on polycrystalline silicon, where it is a main limiting factor of the solar cell efficiency.

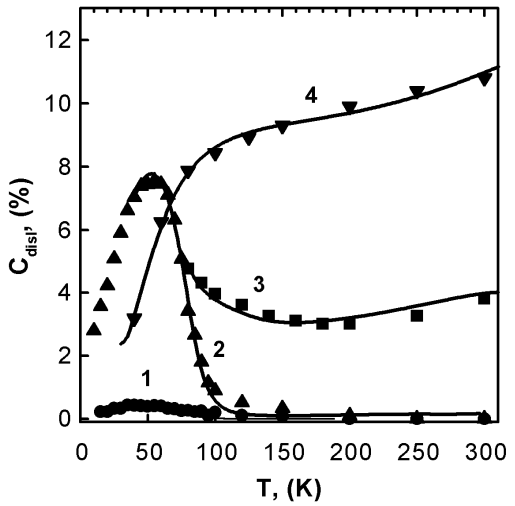

Fig. 12. Temperature dependencies of EBIC contrast $C_{disl}(T)$ of dislocations in Si. Points are experimental data [67], solid curves are calculated using the model [65].

Mostly used experimental tools for probing into carrier recombination at dislocations are the measurement of minority-carrier lifetime (or diffusion length) in case of high dislocation density and electron beam induced current (EBIC) or light beam induced current (LBIC) in case of small dislocation density. The EBIC and LBIC are unique among the electrical characterization methods with respect to a spatial resolution, sufficient to measure at single dislocations. In EBIC or LBIC, the variation of the current at a Schottky contact resulting from excess electrons and holes generated locally by the electron or light beam, is measured, when the specimen area of interest is scanned. The values of current at the dislocation, I_{disl}, and away from it, I_0, are used to define the contrast $C_{disl} = (I_0-I_{disl})/I_0$ of single dislocations. The C_{disl} is proportional to the recombination rate R_{rec} of minority carriers at a given dislocation [66].

Numerous experimental investigations (see, for example [67-72]) show that dislocations in different Si samples often exhibit very different EBIC contrast behaviour $C_{disl}(T)$. It is illustrated in Fig. 12 showing typical examples of $C_{disl}(T)$ measured for dislocations in different samples, but at similar experimental conditions. Such a big difference in recombination rates at dislocations in different samples correlate with the fact, known also from DLTS, that dislocations in different samples have very different concentration of deep intrinsic core defects and impurities.

Good quantitative explanation of experimental results is possible in a model [65], which differs from earlier model [73] in including electronic transitions between 1D-bands E_{De}, E_{Dh} and deep localized states E_{DD} due to overlapping of their wave functions (recombination paths (3) in Fig. 13). Taking these transitions into consideration was found to be really essential for a proper description of the dislocation recombination activity.

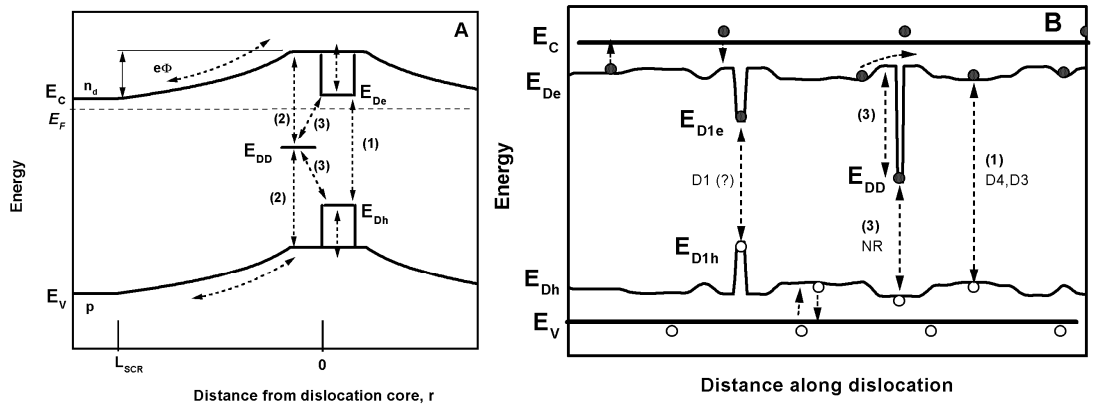

Fig. 13. Charge carrier recombination at dislocations. For clean dislocations the recombination rate is determined by direct recombination of electrons and holes captured by the 1D dislocation bands E_{De}, E_{Dh} (channel (1)). In presence of defects with deep energy level E_{DD}, the carriers captured to 1D-bands can recombine by the paths (3) via this deep level [65].

The recombination rate (1) by transition between 1D-bands is relatively slow. So, the recombination activity of "clean" dislocation is small. However, the recombination can be drastically enhanced by the presence of even small concentration of impurity atoms or core defects at dislocation. In this case it occurs in several steps: capture of free electrons and holes to 1D-bands, their motion along dislocation, then capture from the 1D bands to deep states of defects and recombination. The model allows not only to explain experimentally observed dependencies of recombination rate on temperature and excitation level, but also to estimate the concentration of deep level defects at dislocations.

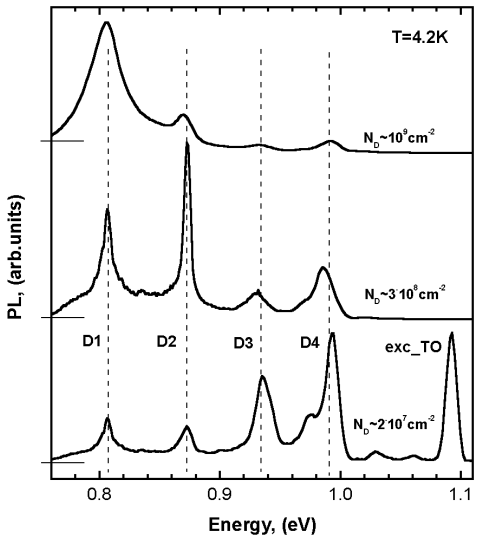

Fig. 14. Spectra of dislocation luminescence in silicon samples with different dislocation densities N_D.
The spectra are normalized to show the same integral intensity.

Dislocation-related luminescence in silicon.

The dislocation-related luminescence consists of four broadened lines (or bands), D1 to D4. Typical photoluminescence spectra measured at T = 4.2 K in samples with different density of dislocations N_D are shown in Fig. 14. The dislocation-related D-band luminescence lines always appear in the presence of dislocations. The relative intensities of D1, D2 and D3, D4 depend on the dislocation density and distribution and can vary strongly in different samples. Usually, at low dislocation density N_D the lines D3, D4 dominate, while at high N_D the D1-line becomes dominating (see Fig. 14).

The polarization of the D-lines emission and their response to uniaxial stress has been utilized to establish their relations to the dislocations. Lines D1 and D2 on the one hand, and lines D3 and D4 on the other, show the similar shifts under

uni-axial stress and therefore have been grouped as pairs, D1/D2 and D3/D4 [74, 75]. From the polarization measurements [76-78] the E-vector of the light for lines D3/D4 was found to be in the glide plane of dislocations and is strongly correlated with the direction of the dislocation Burgers vector. These findings strongly point to the dislocations as radiative centres for D3/D4 lines. For the D1/D2 the situation is more complicated, but still the E-vector is related to the dislocation glide plane, being perpendicular to it. That means that D1/D2 are associated with the dislocation network in some way, but not with point defects or impurity atoms randomly distributed in a bulk.

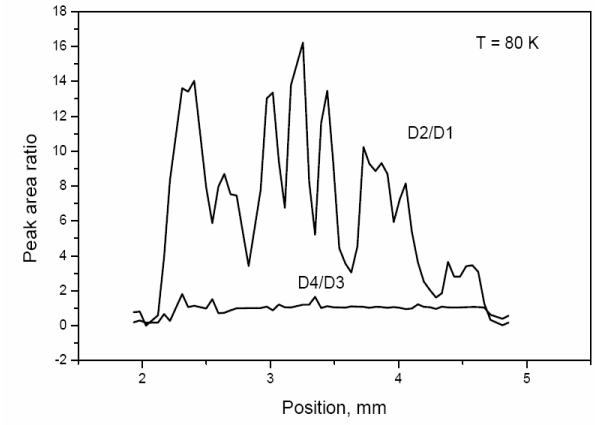

Fig. 15. Spatial distribution of D2/D1 and D4/D3 peak area ratios along a profile measured in multi-crystalline Si at T = 80 K. The ratio D2/D1 varies strongly, whereas D4/D3 remains nearly constant [79].

Investigation of multi-crystalline Si, as used for solar cells, allows studying the relation between the intensity of different D bands radiation from dislocations. As the local density of the dislocations varies in this material from point to point, one can expect also variations in the intensity of the D lines. Profiles of the intensity of the D lines were measured over a distance of a few mm. Fig. 15 shows the corresponding ratios D2/D1 and D4/D3. The intensity ratio of D4/D3 was found to be nearly constant. On the contrary, the D2/D1 ratio scattered strongly [79]. This observation confirms that the lines D3 and D4 have the same origin, while the lines D1 and D2 are not a pair but have different origin.

In spite of many experiments carried out during more than a quarter of century of investigation, the exact origins of the luminescent bands connected with dislocations in silicon are still problems and none of many models advanced for these luminescence lines has been universally accepted.

The nature of D4 and D3 luminescence. Very important experiments for clarification of the nature of D4, D3 lines were the experiments with influence of so-called low temperature / high stress (LTHSD) plastic deformation on the energy position of D4, D3 lines [17, 80].

It was directly shown in [81, 82] by using electron microscopy that if one applies high mechanical stress to already existing 60^o dislocations at $T < 500^oC$ and cools down the sample under stress, this results not only in straightening of the existing dislocations but, in addition, to a large deviation of the staking fault width d between 30^o and 90^o partials in a glide set 60^0-dislocation (see Fig.1) from its equilibrium value d_0. The reason for this is that the glide forces acting to the two partials and their mobility are different. This results in deviation of dislocation dissociation width d of moving dislocations from the equilibrium value d_0. The dissociation is narrowed ($d < d_0$) for those 60^0 dislocations, which have the 30^0 partial moving in front (30/90 dislocations), and is widened for 90/30 dislocations ($d > d_0$).

Using this technique the authors of [17, 80] have found that the energy positions of D4 and D3 lines depend on the distance d between partial dislocations and made a conclusion that D3 and D4 line "families" originate from recombination processes at straight segments of 60^o dislocations. In addition it was concluded that the D3 line is most probably a TO phonon assisted replica of D4.

Taking into account also a very good coincidence between the energy of D4 line and the energy difference E_{De}-E_{Dh}, one can come to suggestion that the D4 line corresponds to no-phonon recombination of electrons in 1D band E_{De} with holes in 1D band E_{Dh}. The D3 line is most probably a TO phonon replica of D4.

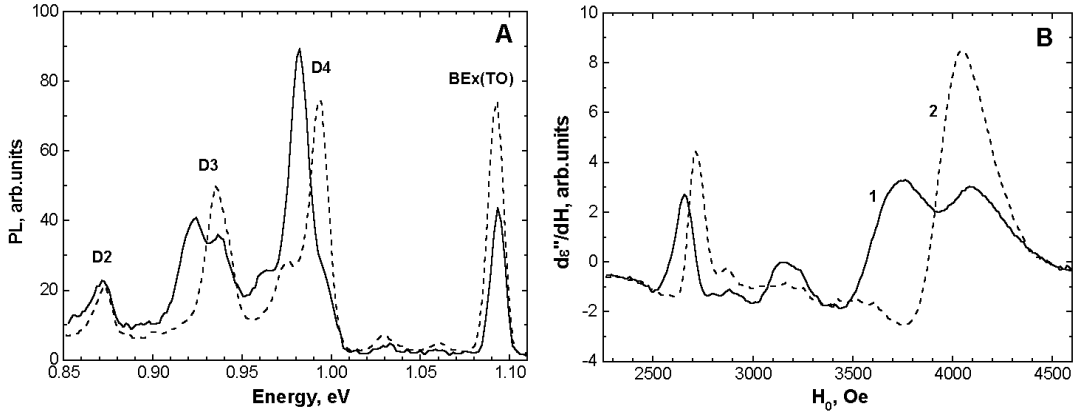

Fig. 16. Luminescence (A) and EDSR spectra (B) in a p-type Si sample with 60° dislocations containing segments with equilibrium ($d = d_0$) and non-equilibrium ($d < d_0$) dissociation (solid curves). The dashed curves show the same sample after annealing at 350°C, leading to $d = d_0$ for all dislocations [55].

The reason for existence of 1D bands at 60° dislocation is its strain field that splits some energy states from the conduction and valence bands of Si crystal. Since the strain field of dissociated 60° dislocation is a superposition of strain fields of 90° and 30° partials (see Fig. 1), it should depend on the dissociation width 'd' of 60° dislocation that is a distance between these two partials. Obviously, change in the distance 'd' between two partial dislocation should result in a change of the total strain field and therefore one can expect deeper positions of 1D bands E_{De}, E_{Dh} for dislocations with smaller 'd'. The change of 'd' should result not only in a shift of luminescence lines D3, D4, but also in a change the g-tensors of electrons and holes in 1D-bands. That was directly proven in [55] by EDSR measurements. The solid curves in Fig. 16 show the spectra of luminescence (A) and of EDSR of holes in 1D-band E_{Dh} (B), measured in a sample cooled down under stress, containing both 60° dislocations with equilibrium ($d = d_0$) and non-equilibrium ($d < d_0$) dissociation (solid curves). Dashed curves in Fig. 16 were measured in the same sample after annealing at 350 °C that makes dissociation of all dislocations equal to equilibrium one ($d = d_0$).

Let us discuss now the temperature dependence of D4, D3 luminescence intensity P_{D4}. It was found that the temperature dependencies of intensity of all lines D1-D4 strongly differ in different samples (see Fig. 17), but at $T < 50$ K the slope of their log(P)-1/T plots always give quite small activation energies E_{loc} in the range from 4 to 14 meV [16, 17]. Using these data, the authors of [16] supposed that the D-luminescence occurs by optical transitions between some deep levels, different for different D-lines, and some very shallow level, with a depth E_{loc} of about 4 to 14 meV. However, this interpretation has many serious weak points. One of them is that due to high density of state in 3D bands the thermal depopulation of such shallow states must occurs at very low temperatures $T <$ 10K, while $P_{D1\text{-}D4}(T)$ experimental curves show this small activation energy up to 30-40 K.

The experimental dependencies of $P_{D4,D3}(T)$ can be quite well understood in the recombination model [65] developed for interpretation of EBIC data. The meaning of a small activation energy $E_{loc} \approx 4$ to 14 meV in this model is the following (see Fig. 13): the motion of electrons and holes in 1D-bands along a dislocation to a distance larger than the localization length L_{min}, needs thermal activation to overcome some random potential fluctuations E_{loc} caused by impurities, kinks and so on. The influence of this small random potential on recombination rate is not significant at $T > 70$K, typical for EBIC measurements.

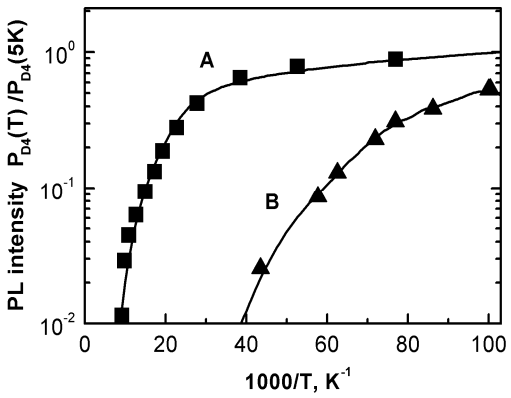

Fig. 17. Temperature dependence of the D4-line photoluminescence intensity in two different samples A and B.
The points are experimental data, while the solid curves are calculated by using model [65].

But at low temperature the average lifetime of carriers in 1D-bands increases with decreasing temperature with activation energy of E_{loc} because the carriers captured to "clean" segments of dislocations need thermal activation to move along dislocation and reach deep recombination defects E_{DD}. Solid curves in Fig. 17 were calculated using model [65]. It was supposed that the intensity of the D4 luminescence is proportional to the recombination rate via channel (1) (see Fig. 13) and the localization length L_{loc} of minority carriers in 1D-bands depends on temperature according to:

$$L_{loc} = L_{max}\, exp(-E_{loc}/k_BT) + L_{min} \qquad (7).$$

Here L_{max}, L_{min} and E_{loc} are some fit parameters. For example, for curve A in Fig.17 the values L_{max} = 89 nm, L_{min} = 6 nm and E_{loc} = 11 meV were used.

The D1-luminescence. The origin of D1 and D2 luminescence is still not really understood. According to the literature, impurity atoms in the dislocation core [83], dislocation jogs [84], segments of dislocations of special types (like Lomer dislocations) appearing due to dislocation reactions, multi-vacancy and/or self-interstitial clusters trapped in the core [85] are typical examples for the origin of the D1 and D2 lines. The prevalence of the D-band luminescence seen in very different samples with different impurity contamination levels gives doubt that metal impurities [83] are primarily responsible for D1 and D2 luminescence. An important fact, which should be taken into account when selecting a model, is that D1 and D2 lines usually dominate the luminescence spectra in samples where dislocations could interact with each other (see Fig. 14). It supports the idea about jogs or Lomer dislocation segments, but also does not contradict the model with multi-vacancy or self-interstitial clusters.

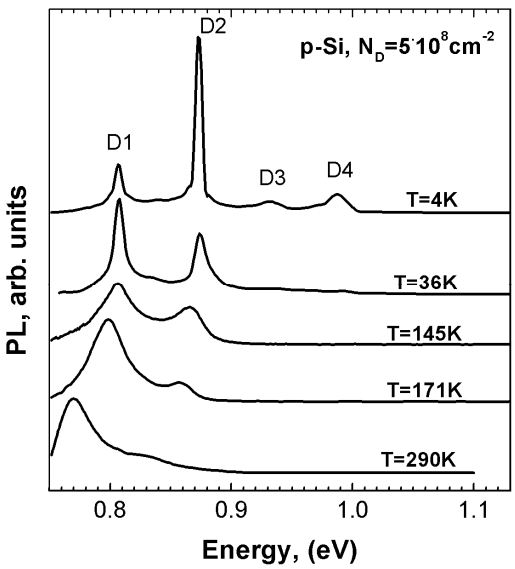

Fig. 18. Typical variation of D-band luminescence spectra with temperature for p-type FZ-Si with a dislocation density $N_D \approx (3\text{-}5)\cdot 10^8$ cm^{-2}. The spectra are normalized to their integral intensity. Please note the absence of the band-to-band luminescence at 1.1 eV [13].

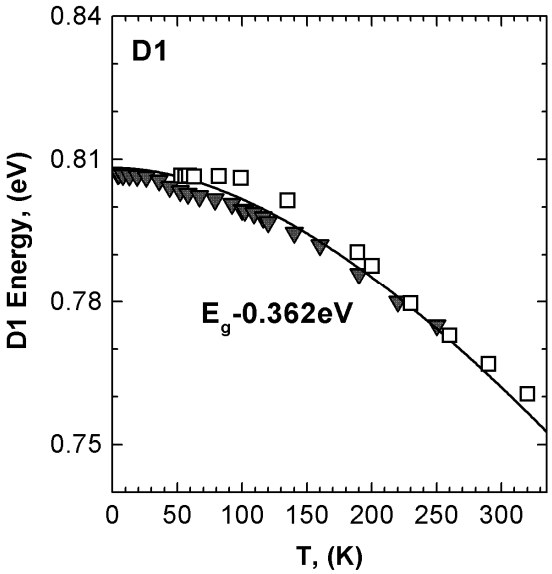

Fig. 19. Variation of the energy position of the D1-line with temperature. Solid symbols – photoluminescense, open symbols – electroluminescence data. The solid curve shows $E_g(T)$ - 0.362 eV, where $E_g(T)$ is the Si band gap.
Note, that positions of D1 can be slightly different in different samples.

At the same time, among all dislocation luminescence lines, the D1 line is most interesting for practical applications. It has a convenient wavelength of about 1.55 μm and it survives up to higher temperature, than the other lines. Fig. 18 shows typical luminescence spectra in a sample with relatively high dislocation density $N_D \approx (3\text{-}5)\cdot 10^8$ cm^{-2} deformed in two glide systems. All dislocation-related lines D1-D4 are present at low temperature, while at high temperatures the broad D1 band gives the main contribution to the luminescence. Fig. 19 shows a typical dependence of the D1 line energy on temperatures. It decreases with increasing temperature approximately in the same way as a Si band-gap $E_g(T)$.

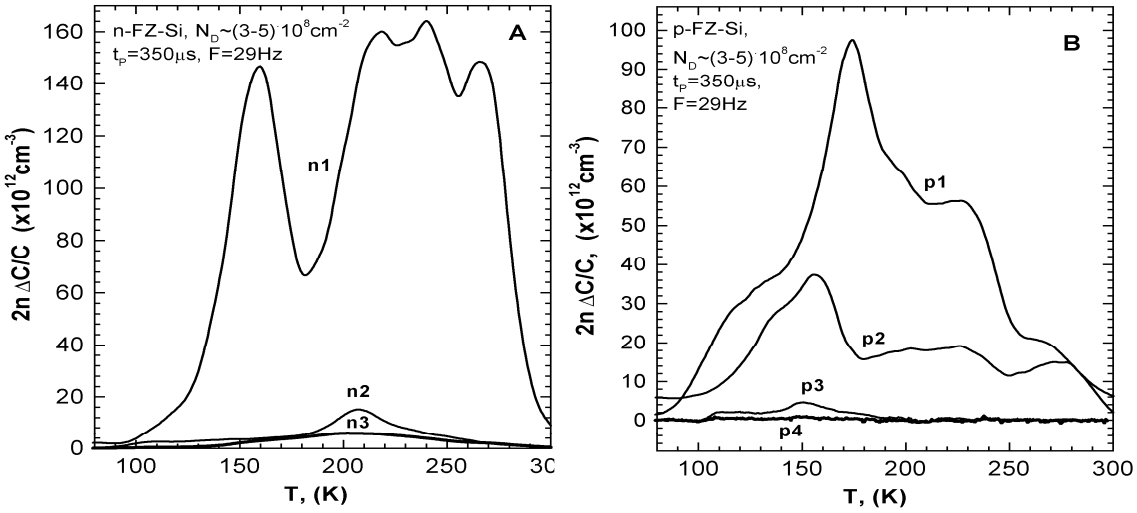

Fig. 20. DLTS spectra in n-type (A) and p-type (B) FZ-Si deformed at 750 °C to produce a dislocation density $N_D \approx (3\text{-}5)\times 10^8$ cm^{-2}.
Curves n1 and p1 were measured just after deformation, n2 and p2 - after ALG at 820 °C for 30-50 min, p3 - after phosphorus diffusion (PDG) 50min at 910 °C, n3 and p4 - after treatment in hydrogen plasma at 270 °C for 60 min [13].

Correlation between D-band luminescence and deep defects detected by DLTS. The quantum efficiency of luminescence in silicon is limited mainly by competing with non-radiative recombination at deep level defects. It should be noted that the band-to-band luminescence, usually observed at the energy of about 1.1 eV in dislocation-free samples, is not detected in highly dislocated samples (see Figs. 17 and 14). It means that if one could increase a non-radiative minority carrier lifetime in silicon with dislocations to a value, comparable with it in dislocation-free silicon, the efficiency of dislocation-related luminescence may become huge. Therefore, one should try to reduce the concentration of non-radiative deep levels defects caused by impurity atoms and core defects at dislocation, for example by a proper annealing, gettering and passivation. Such an attempt was made in [12, 13] where the correlation between efficiency of D1 luminescence and concentration of deep defects detected by DLTS was investigated.

Curves n1 and p1 in Fig. 20 A and B exhibit DLTS spectra in n- and p-type FZ-Si samples deformed at 750°C to a dislocation density of (3-5)x10^8 cm^{-2}. In the as-deformed samples DLTS spectra consist of several overlapping non-uniformly broadened dislocation-related lines well known in literature. The linear density N_{DD} of these states is about $(2\text{-}3)\cdot 10^6$ cm^{-1}. As one can see in Fig. 20, aluminium gettering (AlG) results in a very strong reduction of the DLTS signal to the concentration $N_{DD} \approx 2\cdot 10^5$ cm^{-1}. Subsequent use of phosphorus diffusion gettering (PDG) and hydrogen passivation results in further reduction to $N_{DD} < 10^5$ cm^{-1}.

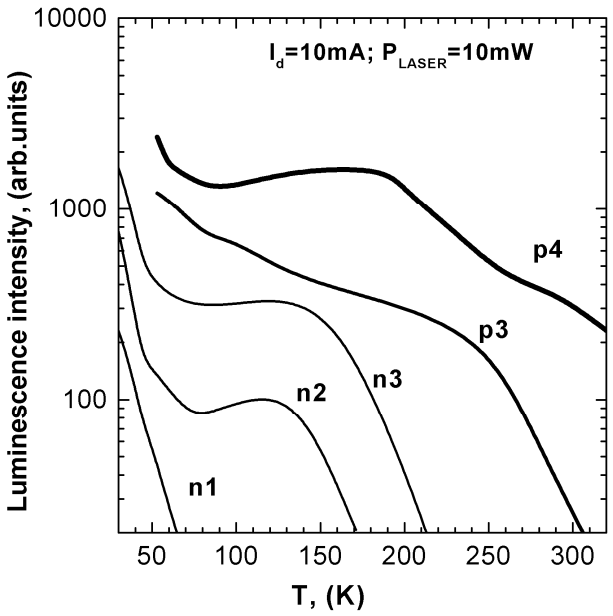

Fig. 21. Temperature dependence of D1+D2 luminescence intensity. Curves (n1-n3) - PL in n-Si (see Fig.20A) with a laser power of 10mW, curves (p3, p4) - EL in p-Si LED (see Fig. 20B) at a forward current of 10mA. The labels at the curves have the same meaning as in Fig. 20.

Fig. 21 shows the temperature dependence of the D1+D2 luminescence intensity in the same samples for which the DLTS spectra are shown in Fig. 20. In n-type samples the luminescence was excited by a 10 mW laser, while in p-type the electro-luminescence (EL) with a forward current of 10 mA was analyzed that was generated by the p-n junction, prepared during PDG. Note, that the excitation level was small enough to be in a linear regime and to avoid saturation of luminescence at $T > 35$ K.

As one can see, a reduction of deep defect concentration N_{DD}, detected by DLTS, results in a dramatic (by orders of magnitude) increasing of D1 luminescence efficiency near room temperature.

An external quantum efficiency η_{ext} of the D1-line electroluminescence from the p-n-junction in sample p4 (see Figs. 20 and 21) was found to be quite high, of about $\eta_{ext} = 0.1\%$ at 300 K. Since no suitable texturing or anti-reflecting coating was used to increase the light extraction from the sample, the internal quantum efficiency η_{int} of this LED is probably significantly higher than the measured external efficiency, since due to the high refraction index of Si only a small fraction of generated photons can leave the sample.

Dependence of D1 and D2 luminescence on excitation level. Fig. 22 shows the light intensity P_{D1} emitted by the p-n junction in sample p4 [13]. The shape of luminescence spectra depends on the forward current I_d. The luminescence spectra in Fig. 22A were normalized to the current value I_d, so, in linear regime they should not depend on I_d. At room temperature the dependence of P_{D1} on I_d is linear up to $I_d = 100$mA (that is about 1 A/cm^2), but at lower temperature it becomes sub-linear with increasing current.

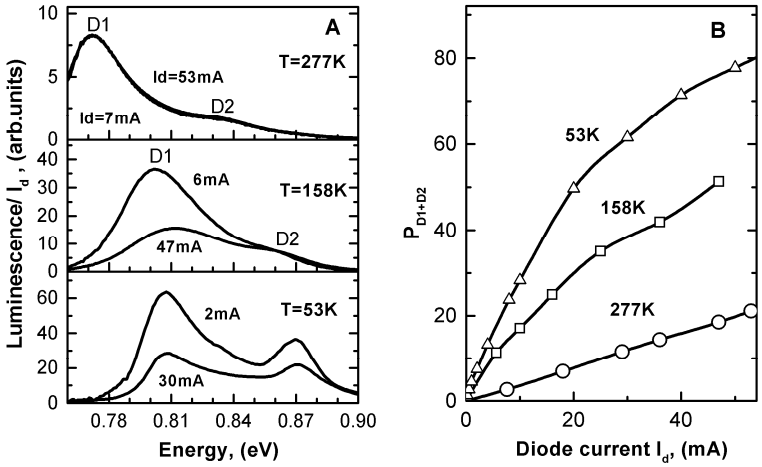

Fig. 22. Dependencies of the overall luminscence intensity (B) and of the luminescence spectra on forward current I_d through the p-n junction, measured at different temperatures.
The spectra (A) are normalized to the value of I_d. of the current.

To our opinion the observed sub-linear behaviour testifies to the saturation caused by approaching of occupation of D1-defects to unity at high concentration n of minority carriers generated by injection from p-n junction. In case of p-Si, n is concentration of electrons, which is proportional to the current density $j_d = I_d/S$ through the p-n$^+$ junction with area S.

One can argue that the dependencies $P_{D1}(I_d)$, shown in Fig. 22B, are quite different from typical dependence expected for saturation in a simple case:

$$P_{D1} \sim N_{D1} \cdot n/(1+B \cdot n) \qquad (8)$$

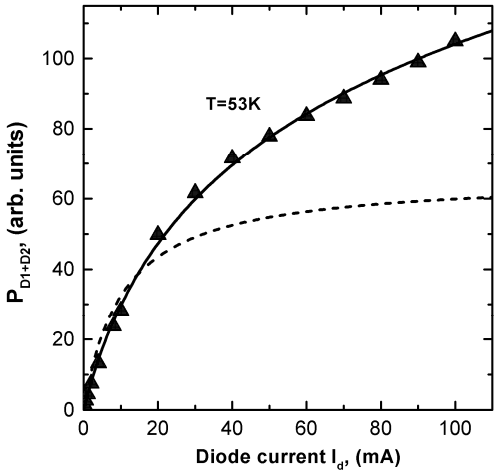

Fig. 23. Dependence of the luminescence intensity on p-n junction current I_d at T = 53 K, points are taken from [13]. The dashed curve is calculated using Eq. 8 and the solid curve is calculated by using Eq. 10.

Here B is some fit parameter, proportional to the product of electron capture cross-section for D1 centres and their lifetime at D1 centres. The dashed curve in Fig. 23 was calculated using Eq. 8, while the triangles the experimental data measured at T = 53 K (see curve "53K" in Fig. 23). Indeed, the experimental dependence obviously does not follow the Eq. 8. However, one should remember that samples used in [13] were much thicker than the minority-carrier diffusion length $L_{nd} = (D_e\tau_{elt})^{1/2}$, where D_e is the diffusion coefficient for electrons and τ_{elt} is their lifetime. In this case, the concentration of electrons n, injected to thick p-type region from p-n^+ junction is not uniform and depends on the distance x from p-n^+ junction as:

$$n(x) \approx (I_d/eS)(\tau_{elt}/L_{nd})\,exp(-x/L_{nd}) \qquad (9)$$

Therefore, to calculate the dependence $P_{D1}(I_d)$, one should integrate the Eq. 8 on x from 0 to infinity with n(x) given by Eq. 9. Taking into account that dislocation concentration N_D and, therefore, concentration of D1-defects N_{D1}, are quite uniform in the samples, we have:

$$P_{D1} \sim \int (N_{D1} \cdot n(x)/(1+B \cdot n(x)))dx \sim N_{D1} L_{nd} \cdot ln(1+bI_d)/b \qquad (10)$$

where b is again a fit parameter. The dependence calculated using Eq. 10 is shown by solid curve in Fig. 23 and it agrees with experimental data quite well.

The fact, that the saturation of the D1 luminescence can be achieved at quite low injection current density, opens a perspective for construction of lasers based on D1-radiation. According to a widely accepted model, the D1 luminescence corresponds to recombination of electrons captured to acceptor level E_{D1e} with holes captured to donor level E_{D1h} of some dislocation-related D1-defects (see Fig. 13B). The saturation of luminescence in such a system means inverse population of these energy levels, necessary for laser generation. Unfortunately, according to estimations made in [13] from photocurrent measurements, the optical absorption coefficient, corresponding to D1-transitions, is quite small for the samples used in [13]. Therefore, to obtain a laser generation one should either use a very high quality optical resonator, or increase significantly the concentration N_{D1} of D1-defects.

Silicon wafer direct bonding: Self-assembly of dislocation networks

Macroscopic plastic deformation is not acceptable to produce dislocations for practical use in microelectronic devices. However, there are many other methods to generate dislocations in a well controlled way and in well-defined places, compatible with standard silicon technology. One of them is a direct bonding of Si wafers, allowing generation of regular dislocation networks. A description of this procedure is presented in a previous publication [22] and in detail within this volume (see M. Reiche, this issue). Here we give only a short description. Another way is to use

dislocation loops that can be formed in a controlled manner by implantation of Si ions and subsequent anneal [86] (see below).

Semiconductor wafer bonding generally refers to a process where two mirror-polished wafers adhere to each other at room temperature without the application of any macroscopic gluing layer or external forces. It is generally assumed that adhesion forces (van der Waals forces, electrostatic Coulomb forces, capillary forces or hydrogen bridge bonds) are the primary bonding forces. At high temperatures, the attractive forces are transformed into Si-Si covalent bonds. Dislocation networks form at the bonding interface as a result of the misorientation of the two wafers for the case of identical materials. Fig. 24 shows as an example a TEM (transmission electron microscopy) plan-views of networks, formed by bonding. In our case of Si (100) / (100), the periodic dislocation network consists of screw dislocations accommodating the twist component and of 60° dislocations compensating the tilt.

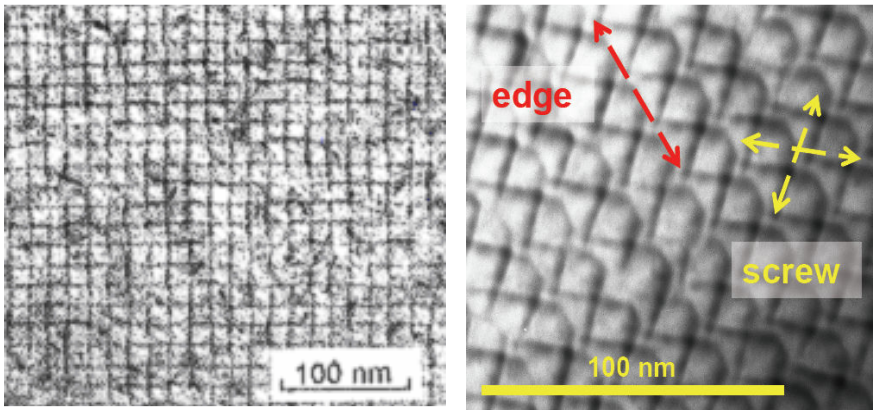

Fig. 24. TEM micrographs (plan view) showing examples of a regular dislocation networks formed by wafer bonding. (a) Left: Network containing screw dislocations. (b) Right: Network containing screw and edge-type dislocations; the directions of these dislocation types are indicated. Note, for this network only the D1-line was detected (see spectrum C in Fig. 25) [89].

The formation of the dislocation network is a self-organized process. The spacing D between the dislocations depends on the angle of misorientation ϑ between both wafers. It can be approximated by the simple relation, $D \sim b / \sin\vartheta$, with b the Burgers vector of the dislocations; for the dislocations in Si, $b = a/2 \langle 110 \rangle$ holds with a = 0.543 nm. Consequently, the distance between the dislocations can be controlled in a wide range by adjusting ϑ. For example, the spacing of dislocations is D ~ 10 nm for a misorientation of about 2° and D ~ 1 µm for a very small misorientation of only 0.02°.

If wafer bonding is carried out on standard Si wafers, the bonded interface is several hundred microns below the surface. Therefore, thinning of one of the wafers is required to place the network close to the surface. It can be done by the so-called smart-cut process [87]. For smart-cut one of the wafers is implanted with hydrogen with a dose $\geq 10^{16}$ at/cm^2 prior to bonding. After bonding an annealing step follows that results in the formation of hydrogen bubbles located parallel to the bonded interface at a depth easily controlled by the implantation energy. The ripening of bubbles causes stress resulting in microcracks and, finally, in the ablation of the thin top layer. Depending on the implantation energy, the thickness of the transferred layer is below 1µm. A further thinning of the layer - to less than 50 nm - can most effectively be done by selective oxidation and removal of the grown oxide.

Luminescence of dislocation networks. Our luminescence measurements provide direct evidence that the wavelength of light emitted from the dislocation network could be tailored to some extent by misorientation of the wafers during bonding procedure.

The structure of a dislocation network, i.e., density and type of the dislocations formed, depends on the misorientation angles for twist and tilt during wafer bonding. The dislocation network can be well reproduced by appropriately adjusting the angles. Fig. 25 demonstrates that the luminescence

spectra strongly correlate with the structure of the dislocation network. Hence, the luminescence spectrum can be tailored by the misorientation angles in a controlled manner [24].

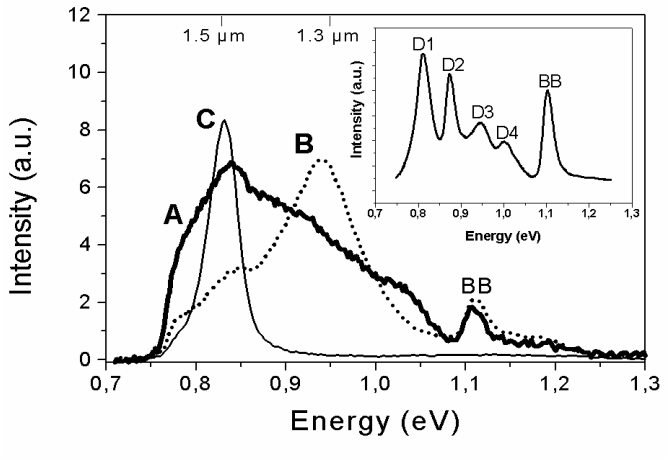

Fig. 25. Example of impact of misorientation/structure on the luminescence spectra of dislocation networks. (A) Twist angle of 9°, dominating D1 line; (B) twist angle of 8.2°, dominating D3 line. Same tilt angle of 0.2° in both cases [89]. (C) Appearance of D1 line for the network shown in Fig. 24. The insert shows a typical spectrum of dislocated Si, exhibiting the D1-D4 lines formed by dislocations and the BB line.

Dislocation-based MOS-LED emitting at 1.5 µm.

Making use of a proper dislocation network positioned close to a MOS tunnelling diode allows to produce a MOS-LED emitting in the IR range around 1.5 µm. Before describing this device we will shortly discuss a MOS-LED on perfect Si without dislocations.

Silicon MOS-LED. Electroluminescence (EL) with emission of the BB line at about 1.1 µm has been demonstrated from a MOS tunnel diode prepared on n-type Si [88]. Under positive gate bias electrons are attracted, building an accumulation layer close to the Si/oxide interface, and a hole current is formed by tunneling through the oxide layer. Also MOS tunnel diodes on p-type Si yield comparable results. Fig. 26 shows the EL spectrum observed at room temperature [89] exhibiting the BB line with an efficiency > 0.1%. As shown in the insert the EL intensity increases sub-linearly with increasing tunneling current. The basic processes in MOS-LEDs on n-type and p-type Si, respectively, are schematically represented in Fig. 27.

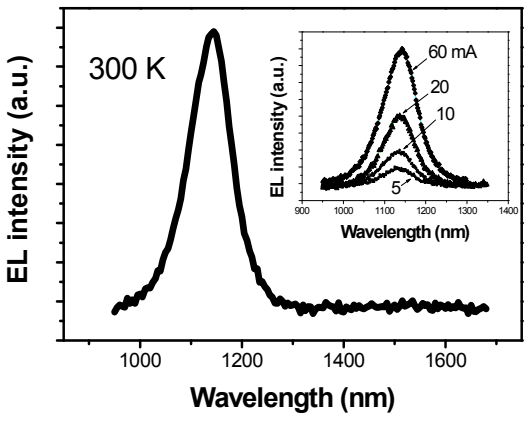

Fig. 26. EL of a MOS tunnel diode on p-Si exhibiting BB luminescence at 300 K with an efficiency > 0.1 %. The insert shows the dependence of the EL signal on the current [89].

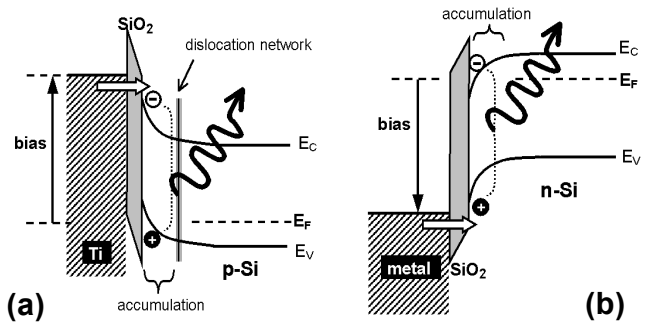

Fig. 27. Scheme of MOS-LED, (a) p-type material with dislocation network, capable of yielding both dislocation and BB luminescence, (b) n-type Si without network yielding BB luminescence only [89].

Dislocation based MOS-LED. When a dislocation network with appropriate structure is positioned near the Si/oxide interface, close to or within the accumulation layer, the radiative recombination is dominated by the dislocation D1 line at about 1.5 μm instead of the BB line. This is clearly seen from the EL spectra shown in Fig. 28. The MOS-LED on p-type Si, with the dislocation network at a depth of about 45 nm, consisted of a 134 nm thick Ti gate (7.9 x 10^{-3} cm^2) deposited on 1.8 nm thick Si oxide, see TEM micrographs shown in Fig. 29. The I-V characteristic is given in the insert of Fig. 28. The tunneling current increases with increasing gate voltage, leading to an enhancement of the EL intensity.

The efficiency of the dislocation-based MOS-LED, estimated from experimentally measured luminescence intensity is of about 0.1% for the 1.5 μm emission at 80 K. Increasing the temperature from 80 to 210 K causes a red-shift of the D1 line and a reduction of the EL intensity / efficiency by a factor of about 2. Increase of temperature to 300 K was found to further reduce the EL efficiency. However, there are several approaches to enhance the room temperature efficiency of MOS-LEDs.

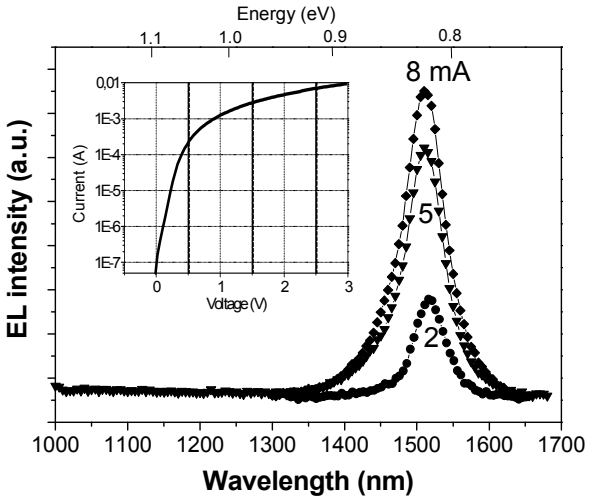

Fig. 28. EL at 80 K of a MOS-LED (gate area of about 7.9 x 10^{-3} cm^2) under negative gate bias with 1.5 μm radiation caused by the dislocation network near the Si/oxide interface. The intensity is found to increase sub-linearly with increasing tunneling current as seen from the spectra measured at 2, 5 and 8 mA, respectively. The insert represents the I-V characteristic of the LED at 300K [89].

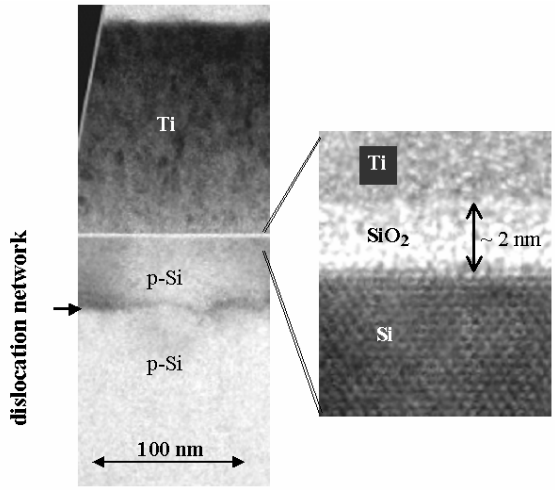

Fig. 29. XTEM of the MOS-LED consisting of a 134 nm Ti layer on 1.8 nm Si oxide. The dislocation network is positioned in a depth of about 45 nm and was fabricated by direct bonding of p-type Si wafers, ρ ~ 10 Ωcm, with (100) orientation [89].

Prospects for future improvements of the MOS-LED. We suppose that elimination of non-radiative recombination channels, such as states at the Si/oxide interface and deep states at dislocations caused by metal impurity contaminations, will significantly improve the efficiency and sufficient 1.5 μm luminescence at 300 K is achievable with dislocation networks. Below we will show that a D1-line efficiency > 0.3% at 300 K was demonstrated already for a p-n LED containing a dislocation network [90].

Additional improvement of efficiency of MOS-LED can be achieved by utilization of gate dielectrics with smaller band-gap (e.g. Hf oxide) and by using stacks of multiple parallel networks. Moreover, a bias voltage applied to the network can also enhance the D-line emission. The influence of a bias voltage to the intensity of cathodoluminescence was demonstrated mode (Fig. 30). We also observed that, for the same structure of the dislocation network, the intensity of the D1 luminescence is significantly enhanced (about three times) by a trace of oxygen accommodated at

the bonded interface [89]. Oxygen exhibits this positive influence when its content is just above the SIMS detection limit and when no Si oxide precipitates are observed at the bonded interface. Hence, controlled placement of a trace of oxygen (Si oxide) before wafer direct bonding may help to increase the efficiency of a dislocation-based light emitter.

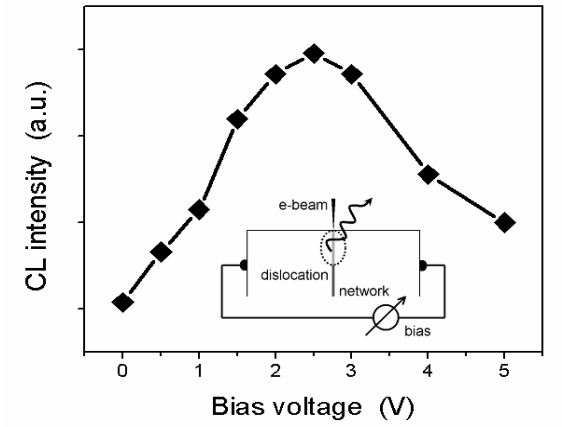

Fig. 30. Enhancement of D-line CL emission caused by a bias applied to the dislocation network. The maximum intensity appears at about 2.5 V. The insert represents the sample configuration [89].

Electroluminescence of dislocations due to forward biased p-n junctions

A forward biased p-n junction generates excess electron and holes in a region of the semiconductor material surrounding the junction. A part of these carriers recombines radiatively. For nearly perfect silicon the band-to-band line at 1.1 μm was detected with an efficiency of the EL of about 2% at room temperature, e.g. [11] and references therein. A detailed description is given by N. Sobolev in this issue.

If dislocations are located close to the p-n junction D-band luminescence appears in the EL spectrum, e.g. [12, 89]. Below we report EL caused by a dislocation network and by dislocation loops, both of which can be produced in a controlled manner.

EL at 1.5 μm caused by a dislocation network. A schematic view of a p-n LED consisting of a p-n junction and a dislocation network is shown in Fig. 31a. An EL spectrum measured at room temperature is shown in Fig. 31b. The spectrum contains both, the BB-line and the D1-line exhibiting an internal efficiency > 0.3%. The distance between the p-n junction and the network, which was formed by bonding of p-type (100) Si wafers, is about 2 μm. Accordingly, a part of the radiative recombination appears in the defect-free Si material causing the BB-line. A network in n-type Si is expected to yield even a higher efficiency. More details are be given in [90].

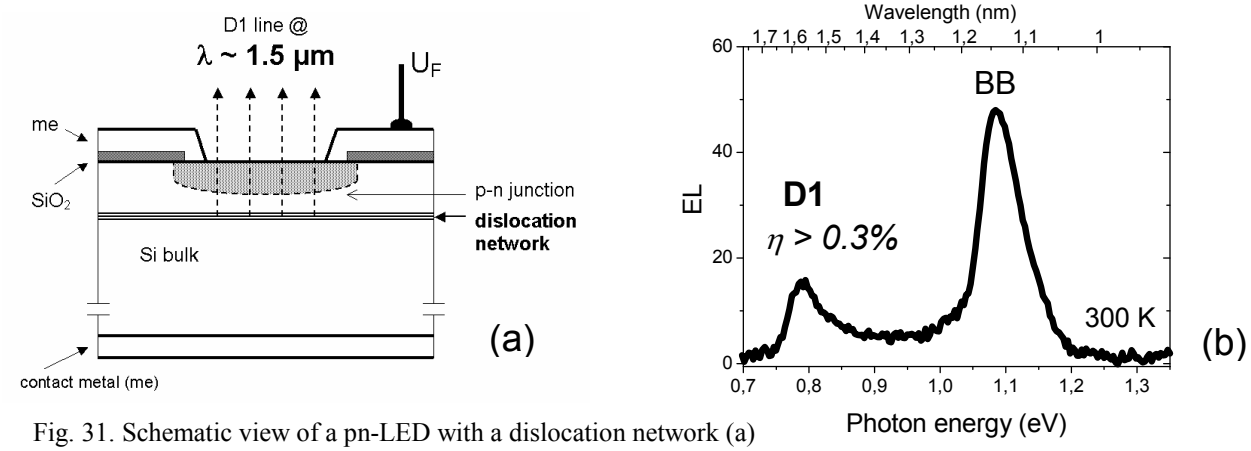

Fig. 31. Schematic view of a pn-LED with a dislocation network (a) and EL spectrum at 300K exhibiting > 0.3% efficiency for the D1-line (b).

EL at 1.5 µm caused by dislocation loops formed by Si implantation. Diodes formed by boron diffusion into n-type Si were implanted with 10^{15} Si^+ ions per cm^2 with energies 200 and 450 keV and subsequently annealed at 950 °C for 20 min in nitrogen ambient to form dislocation loops, see [91]. Fig. 32 represents a device scheme and a XTEM micrograph showing the loops. The dislocation bands were located close to the p-n junction in the B doped p^+-layer and in the n-substrate, respectively. The EL spectrum of the diode exhibits the dislocation related peaks D1, D2 and D3, where D1 dominates, see Fig. 33.

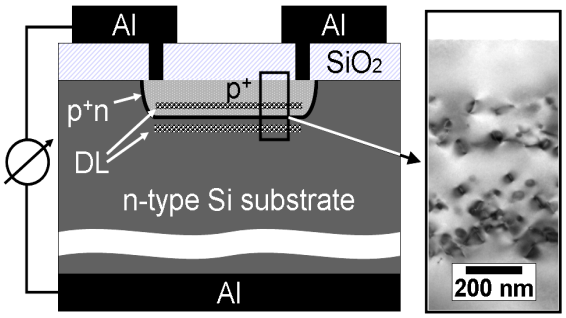

Fig. 32. Schematic illustration of the cross-section of the p-n diode formed by B diffusion into n-type Si. Two bands of dislocation loops (DL) formed by Si implantation are shown in the XTEM micrograph [86].

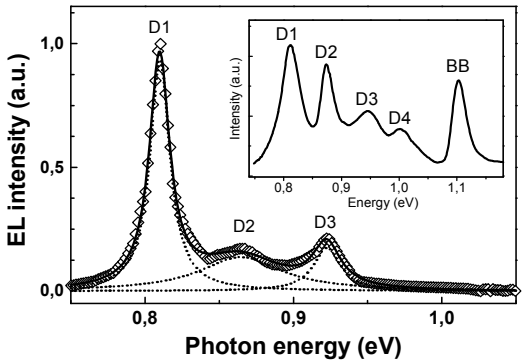

Fig. 33. EL spectrum detected at 30 K from a LED containing dislocation loops. For comparison, a typical luminescence spectrum of dislocated Si is given in the inset [92].

Influence of electric field on spectral position of the dislocation D1-luminescence: Stark effect at light emitting dislocations.

In the structure shown in Fig. 32, the dislocations are located in a strong electric field formed by the depletion region of a p-n-junction. This may result in some energy shift of levels, caused by Stark-effect. A shift of the D1 peak energy with variation of voltage applied to p-n-junction was observed in [92] in a wide temperature range between 30 K and 300 K. A thermal mechanism of the shift, related to the increased carrier injection, was excluded because the position of the BB peak, which is also sensitive to the temperature, did not change upon variation of a voltage at p-n-junction. Fig. 34 shows the influence of reverse bias voltage applied to p-n-junction on the spectral position of the D1 photoluminescence excited by 476 nm laser illumination. One can see, that increase of electric field F results in a red shift of D1 line, while the position of free exciton remains unchanged. Fig.35 shows the dependence of D1 peak position on electric field in p-n-junction. It was proposed in [92] that the observed shift of D1 peak position is related to quadric Stark effect [93], which implies a parabolic shift in the luminescence energy E_{ex} depending on an electric field: $E_{ex} = E_{ex}(0) - \alpha F^2$, where $E_{ex}(0)$ is the energy of excitonic transition at $F = 0$ and α is a characteristic coefficient. From the data shown in Fig. 35 one can find $E_{ex}(0) = 795$ meV and $\alpha = 0.0186$ meV/(kV/cm)^2.

The Stark effect on dislocations can be used for a controlled tuning of the spectral position of the D1 light. If the spectral shift can be performed in a sufficiently short time, a combination of an electro-optical modulator and the light emitter within one device can be realized.

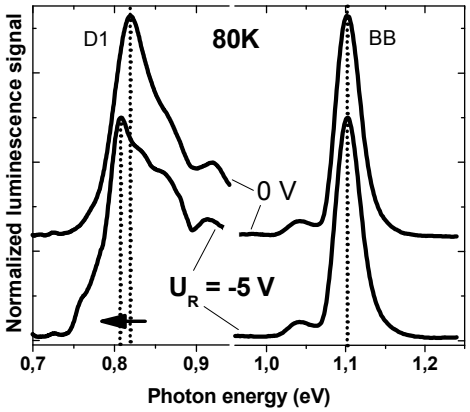

Fig.34. The PL spectra measured for dislocations in p-n-junction under revers bias of 0 and -5V. The PL was excited by laser with a wavelength of 476nm [63].

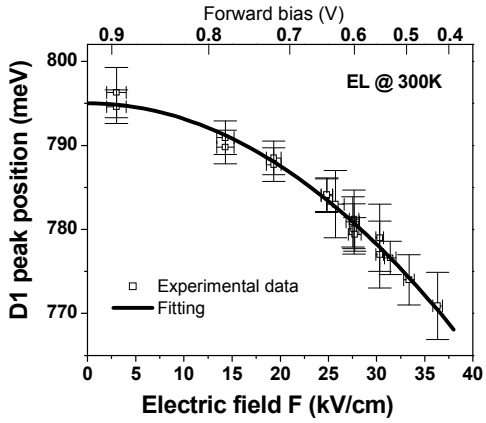

Fig.35. The position of D1 line depending on the electric field in p-n-junction, measured at 300K [92].

Summary

The D1 luminescence related to dislocations in silicon is a promising candidate for silicon-based light emitting diodes (LED) with a light wavelength of about 1.55 μm, suitable for in-chip optical interconnects. Novel Si LEDs based on dislocation networks fully compatible with Si technology have been demonstrated. According to our estimates and the supposed improvements it offers the capability for efficiency around 1% at room temperature. We consider the proposed dislocation network-based LED a promising concept for the realization of a Si-based on-chip light emitter. Moreover, the appearance of the Stark effect may allow to combine modulator and light emitter and within one device.

References

[1] L. Pavesi, *J. Phys.: Condens. Mater.* **15**, R1169 (2003)

[2] A. Liu, R. Jones, L. Liao, D. Samara-Rubio, D. Rubin, O. Cohen, R. Nicolaescu, M. Pannicia, *Nature* **42**7, 615 (2004)

[3] M. Oehme, J. Werner, M. Jutzi, G. Wöhl, E. Kasper, M. Berroth, *Thin Solid Films* **50**8, 393 (2006)

[4] H. Ennen, G. Pomrenke, A. Axmann, K. Eisele, W. Haydl, J. Schneider, *Appl. Phys. Lett.* **46**, 381 (1985)

[5] B. Zheng, J. Michel, F.Y.G. Ren, L.C. Kimerling, D.C. Jacobson, J.M. Poate, *Appl. Phys. Lett.* **64,** 2842 (1994)

[6] G. Franzo, S. Boninelli, D. Pacifici, F. Priolo, F. Icona, C. Bongiorno, *Appl. Phys. Lett.* **82**(22), 3871 (2003)

[7] J. Chevrier, J.Y. Natoli, I. Berbezier, A. Ronde, J. Derrien, *Solid State Phenomena* Vols. **32-33**, 39 (1993)

[8] D. Leong, M. Harry, K.J. Reeson, K.P. Homewood, *Nature* **387**, 686 (1997)

[9] M.A. Lourenco, M.S.A. Siddiqui, R.M. Gwilliam, G. Shao, P. Homewood, *Physica E* **16**, 387 (2003)

[10] N.D. Zakharov, V.G. Talaev, P. Werner, A.A. Tonikikh, G.E. Cirlin, *Appl.Phys.Lett.* **83**, 3084 (2003)

[11] M. Kittler, T. Arguirov, A. Fischer, W. Seifert, *Opt. Mater.* **27**, 967 (2005)

[12] V. Kveder, M. Badylevich, E. Steinman, A. Izotov, M. Seibt, W. Schröter, *Appl. Phys. Lett.* **84**, 2106 (2004)

[13] V. Kveder, M. Badylevich, W. Schröter, M. Seibt, E. Steinman, A. Izotov**,** *Phys. Stat. Sol.* (a) **202**, 901 (2005)

[14] N.A. Drozdov, A.A. Patrin, V.D. Tkachev, *Sov. Phys. JETP Lett.* **23**, 597 (1976)

[15] M. Suezawa, K. Sumino, *Phys. Stat. Sol.* (a) **78**, 639 (1983)

[16] M. Suezawa, Y. Sasaki, K. Sumino, *Phys. Stat. Sol.* (a) **79**, 173 (1983)

[17] R. Sauer, J. Weber, J. Stolz, E.R. Weber, K.-H. Küsters, H. Alexander, *Appl.Phys.* **A 36**, 1 (1985)

[18] V. Higgs, E.C. Lightowlers, S. Tajbakhsh, *Appl. Phys. Lett.* **61**, 1087 (1992)

[19] E.Ö. Sveinbjörnsson, J. Weber, *Appl. Phys. Lett.* **69**, 2686 (1996)

[20] V.V. Kveder, E.A. Steinman, S.A. Shevchenko, H.G. Grimmeiss, *Phys.Rev. B* **51**, 10520 (1995)

[21] T. Hoang, P. LeMinh, J. Holleman, J. Schmitz, *IEEE Electron Device Lett.* **28**(5), 384 (2007)

[22] M. Reiche, K. Scheerschmidt, D. Conrad, R. Scholz, A. Pößl, U. Gösele, K.N. Tu, *Inst. Phys. Conf. Ser.* **15**7, 447 (1997)

[23] E.O. Sveinbjörnsson, S. Bengtsson, J. Weber, N. Keskitalo, *Electrochem. Society Proc. Vol.* **97-36**, 264 (1998)

[24] M. Kittler, M. Reiche, T. Arguirov, W. Seifert, X. Yu, *IEDM Tech. Digest 200*5, 1027 (2005)

[25] W. Schröter, H. Cerva, *Solid State Phenomena* **85-86**, 67 (2002)

[26] F.D. Wöhler, H. Alexander, W. Sander, *J. Phys. Chem . Solids* **31**, 1381 (1970)

[27] V.A. Grazhulis and Yu.A. Osipian, *Sov. Phys. JETP* **31**, 677 (1970)

[28] V.V. Kveder, Yu.A. Osipian, M.N. Zolotukhin, *Sov. Phys. JETP* **53**, 160 (1981)

[29] W. Schröter, J. Kronewitz, U. Gnauert, F. Riedel, M. Seibt, *Phys. Rev.* B **52** 13726 (1995)

[30] W. Schröter, H. Hedemann ,V. Kveder, F. Riedel, *J. Phys.: Condens. Matter* **14**, 13047–13059 (2002)

[31] V.V. Kveder, Yu.A. Osipian, W. Schröter, G. Zoth, *Phys.Stat. Sol.* (a), **72**,701-713, (1982)

[32] V. Kveder, V. Orlov, M. Khorosheva, M. Seibt, *Solid State Phenomena,* Vols. **131-133**, 175 (2008)

[33] J.R. Patel, L.C. Kimerling, *J. Physique* **40**, C6-67 (1979)

[34] P. Omling, E.R. Weber, L. Montelius, H. Alexander, J. Michel, *Phys. Rev.* B **32**, 6571 (1985)

[35] D. Cavalcoli, A. Cavallini, E. Gombia, *Phys. Rev.* B, **56**, 10208, (1997)

[36] M. Kittler, C. Ulhaq-Bouillet, V. Higgs, *Mater. Sci. Forum* **196-201**, 383 (1995)

[37] W. Schröter, V. Kveder, H. Hedemann, *Solid State Phenomena* **82-84**, 213 (2002)

[38] V. Kveder, W. Schröter, M. Seibt, A. Sattler, *Solid State Phenomena* **82-84**, 361 (2002)

[39] K. Knobloch, M. Kittler, W.Seifert, *J .Appl. Phys.* **93**, 1069 (2003)

[40] V.V. Kveder, Yu.A. Osipian, I.R. Sagdeev, A.I. Shalynin, M.N. Zolotukhin, *Phys. Stat. Sol.* (a), **87**, 657 (1985)

[41] V.V. Kveder, Yu.A. Osipian, M.N. Zolotukhin, Sov. *Phys. JETP* **55**(6), 1189 (1982)

[42] J.I. Hanoka, C.H. Seager, D.J. Sharp, J.K.G. Panitz, *Appl. Phys. Lett.* **42**, 618 (1983)

[43] V.V. Kveder, Yu.A. Osipian, "Interaction of hydrogen with dislocations in Si", pp. 395-398 in "Dislocations in Solids" - Yamada Science Foundation, 1985

[44] A. Castaldini, D. Cavalcoli, A. Cavallini, S. Pizzini, *Phys. Rev. Lett.* **95**, 076401 (2005)

[45] M. Brohl, H. Alexander, *Inst. Phys. Conf. Ser.* **104**, 163 (1989)

[46] M. Brohl, M.D. Dressel, H.W. Helberg, H. Alexander, *Phil. Mag.* B **61**, 97 (1990)

[47] V.V. Kveder, Yu.A. Osipian, A.I. Shalynin, *Sov. Phys. JETP* **61**(1), 182 (1985)

[48] A. Bazhenov, V. Kveder, L. Krasilnikova, K. Rezchikov, *Phys. Stat. Sol.* (a) **137**, 321 (1993)

[49] V.V. Kveder, Yu.A. Osipian, A.I. Shalynin, *JETP Lett.* **40**(1), 729 (1984)

[50] V.V. Kveder, V.Ya. Kravchenko, T.R. Mchedlidze, Yu.A. Osipian, D.E. Khmelnizkii, A.I. Shalynin, *JETP Lett.* **43**(4), 255 (1986)

[51] V.V. Kveder, A.E. Koshelev, T.R. Mchedlidze, Yu.A. Osipian, A.I. Shalynin, *Sov. Phys. JETP* **68**(1), 104 (1989)

[52] M. Wattenbach, C. Kisielowski-Kemmerich, H. Alexander, V.V. Kveder, T.R. Mchedlidze, Yu.A. Osipian, *Phys. Stat. Sol.* (b), **158**, K49 (1990)

[53] V.V. Kveder, *Solid State Phenomena* **32-33**, 279 (1993)

[54] V. Kveder, T. Sekiguchi, K. Sumino, *Phys.Rev.* B **51**(23), 16721 (1995)

[55] V.V. Kveder, A.I. Shalynin, E.A. Steinman, A.N. Izotov, *JETP* **83**(4), 829 (1996)

[56] V.V. Kveder, A.I. Shalynin, E.A. Steinman, A.N. Izotov, *Solid State Phenomena* **57-58**, 299 (1997)

[57] G. Dresselhaus, *Phys. Rev.* **100,** 580 (1955)

[58] E.I. Rashba, *Sov. Phys. Solid State* **2,** 1109 (1960)

[59] K. Wessel, H. Alexander, *Phil. Mag.* **35**, 1523 (1977)

[60] M. Brohl, H.Alexander, "Structure and Properties of Dislocations in Semiconductors", edited by S.G. Roberts, D. B.Holt and P.R. Wilshaw, IOP Conf. Proc. No. 104 (Institute of Physics, London, 1989), p.163

[61] M. Kittler, M.Reiche, W. Seifert, X. Yu, T. Arguirov, O.F. Vyvenko, T. Mchedlidze, T. Wilhelm, *ECS Transactions* **3**(4), 429 (2006)

[62] X. Yu, T. Arguirov, M. Kittler, W. Seifert, M. Ratzke, M. Reiche, *Mater. Sci. Semicond. Processing* **9**, 96 (2006)

[63] M. Kittler, M. Reiche, T. Arguirov, T. Mchedlidze, W. Seifert, O.F. Vyvenko, T. Wilhelm, X. Yu, *Solid State Phenomena* Vols. **131-133**, 289 (2008)

[64] Y. Ishikawa et al., *MRS Proc.* Vol. **E6.5.1**, 864 (2005)

[65] V. Kveder, M. Kittler, W. Schröter, *Phys. Rev.* B **63**, 115208 (2001)

[66] C. Donolato in "Point and Extended Defects in Semiconductors", eds. G. Benedek, Cavallini, W. Schröter, Plenum New York (1989) p. 225

[67] M. Kittler, C. Ulhaq-Bouillet, V. Higgs, *J. Appl. Phys.* **78**, 4573 (1995)

[68] M. Kittler, W. Seifert, *Scanning Microscopy* **15**, 316 (1993)

[69] M. Kittler, W. Seifert, V. Higgs, *Phys. Stat. Sol.* (a) **137**, 327 (1993)

[70] K. Knobloch, M. Kittler, W. Seifert, J.J. Simon, I. Perichaud, *Solid State Phenomena* **63-64**, 105 (1998)

[71] S. Kusanagi, T. Sekiguchi, B. Shen, K. Sumino, *Mater. Sci. Technology* **11**, 685 (1995)

[72] B. Shen, T. Sekiguchi, K. Sumino, *Jpn. J. Appl. Phys.* **35**, 3301 (1996)

[73] P.R. Wilshaw, G.R. Booker, *Inst. Phys. Conf. Ser.* **76**, 329 (1985)

[74] N. A. Drozdov, A. A. Patrin, V. D. Tkachev, *Phys. Stat. Sol.* (b) **83**, K137 (1977)

[75] R. Sauer, J. Weber, J. Stolz, E.R. Weber, K.-H. Küsters, H. Alexander, *Appl. Phys.* A **36**, 1 (1985)

[76] J. Weber, *Solid State Phenomena* **37-38**, 13 (1994)

[77] K. Weronek, PhD Thesis Stuttgart, Germany 1992

[78] A.N. Izotov, E.A. Steinman, *Sov. Phys. Solid State* **28**, 567 (1986)

[79] T. Arguirov, PhD thesis Cottbus, Germany 2007

[80] R. Sauer, Ch. Kisielowski-Kemmerich, H. Alexander, *Phys. Rev. Lett.* **57**, 1472 (1986)

[81] K. Wessel, H. Alexander, *Phil. Mag.* **35**, 1523 (1977)

[82] H. Alexander, H. Eppenstein, H. Gottschalk, S. Wendler, *J. Microsc.* **118**, 13 (1980)

[83] V. Higgs, E.C. Lightowlers, E.A. Fitzgerald, Y.-H. Xie, J. Silverman, *J. Appl. Phys.* **73**, 1952 (1993)

[84] G.P. Watson, J.L. Benton, Y.H. Xie, E.A. Fitzgerald, *J. Appl. Phys.* **83**, 3773 (1998).

[85] R. Jones, B.J. Coomer, J.P. Goss, S. Öberg, P.R. Briddon, *Phys. Stat. Sol. (b)* **222**, 133 (2000)

[86] T. Hoang, J. Holleman, P. LeMinh, J. Schmitz, T. Mchedlidze, T. Arguirov, M. Kittler, *IEEE Transactions on Electron Devices* **54**(8), 1860 (2007)

[87] B. Aspar, M. Bruel, H. Moriceau, C. Maleville, T. Poumeyrol, A.M. Papon, A. Claverie, G. Benassayag, A.J. Auberton-Herve, T. Barge, *Microelectron. Eng.* **36**, 233 (1997)

[88] C.W. Liu, M.H. Lee, M.-J. Chen, I.C. Lin, C.-F. Lin, *Appl. Phys. Lett.* **76**, 1516 (2000)

[89] M. Kittler, M. Reiche, X. Yu, T. Arguirov, O.F. Vyvenko, W. Seifert, T. Mchedlidze, G. Jia, T. Wilhelm, *Tech. Digest IEDM 2006*, pp. 845-848

[90] M. Kittler, M. Reiche, W. Seifert, X. Yu, T. Arguirov, O.F. Vyvenko, T. Mchedlidze, T. Wilhelm, *ECS Transactions* **3**(4), 429 (2006)

[91] M. Kittler, M. Reiche, T. Mchedlidze et al., 'Photonics West' to be held in San Jose, Jan. 2008, Proc. SPIE "Silicon Photonics III", manuscript # 6898-12

[92] T. Mchedlidze, T. Arguirov, M. Kittler, T. Hoang, J. Holleman, J. Schmitz, *Appl. Phys. Lett.* **91**, 201113 (2007)

[93] D.A.B. Miller, D.S. Chemla, T.C. Damen, A.C. Gossard, W. Wiegmann, T.H. Wood, C.A. Burrus, *Phys. Rev.* B **32**, 1043 (1985)

Advances in Light Emitting Materials
10.4028/www.scientific.net/MSF.590

Dislocations in Silicon and D-Band Luminescence for Infrared Light Emitters
10.4028/www.scientific.net/MSF.590.29

DOI References
[1] L. Pavesi, J. Phys.: Condens. Mater. 15, R1169 (2003)
doi:10.1088/0953-8984/15/26/201
[2] A. Liu, R. Jones, L. Liao, D. Samara-Rubio, D. Rubin, O. Cohen, R. Nicolaescu, M. Pannicia, Nature 427, 615 (2004)
doi:10.1038/nature02310
[3] M. Oehme, J. Werner, M. Jutzi, G. Wöhl, E. Kasper, M. Berroth, Thin Solid Films 508, 393 (2006)
doi:10.1016/j.tsf.2005.06.106
[4] H. Ennen, G. Pomrenke, A. Axmann, K. Eisele, W. Haydl, J. Schneider, Appl. Phys. Lett. 46, 381 (1985)
doi:10.1063/1.95639
[6] G. Franzo, S. Boninelli, D. Pacifici, F. Priolo, F. Icona, C. Bongiorno, Appl. Phys. Lett. 82(22), 3871 (2003)
doi:10.1016/j.mseb.2003.08.045
[7] J. Chevrier, J.Y. Natoli, I. Berbezier, A. Ronde, J. Derrien, Solid State Phenomena Vols. 32- 33, 39 (1993)
doi:10.4028/www.scientific.net/SSP.32-33.39
[8] D. Leong, M. Harry, K.J. Reeson, K.P. Homewood, Nature 387, 686 (1997)
doi:10.1038/42667
[11] M. Kittler, T. Arguirov, A. Fischer, W. Seifert, Opt. Mater. 27, 967 (2005)
doi:10.1016/j.optmat.2004.08.045
[12] V. Kveder, M. Badylevich, E. Steinman, A. Izotov, M. Seibt, W. Schröter, Appl. Phys. Lett. 84, 2106 (2004)
doi:10.1063/1.1689402
[13] V. Kveder, M. Badylevich, W. Schröter, M. Seibt, E. Steinman, A. Izotov, Phys. Stat. Sol. (a) 202, 901 (2005)
doi:10.1002/pssa.200460512
[15] M. Suezawa, K. Sumino, Phys. Stat. Sol. (a) 78, 639 (1983)
doi:10.1002/pssa.2210780231
[16] M. Suezawa, Y. Sasaki, K. Sumino, Phys. Stat. Sol. (a) 79, 173 (1983)
doi:10.1002/pssa.2210790119
[17] R. Sauer, J. Weber, J. Stolz, E.R. Weber, K.-H. Küsters, H. Alexander, Appl.Phys. A 36, 1 (1985)
doi:10.1007/BF00616453
[18] V. Higgs, E.C. Lightowlers, S. Tajbakhsh, Appl. Phys. Lett. 61, 1087 (1992)
doi:10.1063/1.107676
[20] V.V. Kveder, E.A. Steinman, S.A. Shevchenko, H.G. Grimmeiss, Phys.Rev. B 51, 10520 (1995)
doi:10.1103/PhysRevB.51.10520
[21] T. Hoang, P. LeMinh, J. Holleman, J. Schmitz, IEEE Electron Device Lett. 28(5), 384 (2007)
doi:10.1109/LED.2007.895415

[24] M. Kittler, M. Reiche, T. Arguirov, W. Seifert, X. Yu, IEDM Tech. Digest 2005, 1027 (2005)
doi:10.1109/IEDM.2005.1609533
[32] V. Kveder, V. Orlov, M. Khorosheva, M. Seibt, Solid State Phenomena, Vols. 131-133, 175 (2008)
doi:10.4028/www.scientific.net/SSP.131-133.175
[33] J.R. Patel, L.C. Kimerling, J. Physique 40, C6-67 (1979)
doi:10.1051/jphyscol:1979614
[34] P. Omling, E.R. Weber, L. Montelius, H. Alexander, J. Michel, Phys. Rev. B 32, 6571 (1985)
doi:10.1103/PhysRevB.32.6571
[35] D. Cavalcoli, A. Cavallini, E. Gombia, Phys. Rev. B, 56, 10208, (1997)
doi:10.1103/PhysRevB.56.10208
[36] M. Kittler, C. Ulhaq-Bouillet, V. Higgs, Mater. Sci. Forum 196-201, 383 (1995)
doi:10.4028/www.scientific.net/MSF.196-201.383
[37] W. Schröter, V. Kveder, H. Hedemann, Solid State Phenomena 82-84, 213 (2002)
doi:10.4028/www.scientific.net/SSP.82-84.361
[38] V. Kveder, W. Schröter, M. Seibt, A. Sattler, Solid State Phenomena 82-84, 361 (2002)
doi:10.4028/www.scientific.net/SSP.82-84.361
[39] K. Knobloch, M. Kittler, W.Seifert, J .Appl. Phys. 93, 1069 (2003)
doi:10.1063/1.1532938
[40] V.V. Kveder, Yu.A. Osipian, I.R. Sagdeev, A.I. Shalynin, M.N. Zolotukhin, Phys. Stat. Sol. (a), 87, 657 (1985)
doi:10.1002/pssa.2210870230
[44] A. Castaldini, D. Cavalcoli, A. Cavallini, S. Pizzini, Phys. Rev. Lett. 95, 076401 (2005)
doi:10.1103/PhysRevLett.95.076401
[46] M. Brohl, M.D. Dressel, H.W. Helberg, H. Alexander, Phil. Mag. B 61, 97 (1990)
doi:10.1080/13642819008208654
[48] A. Bazhenov, V. Kveder, L. Krasilnikova, K. Rezchikov, Phys. Stat. Sol. (a) 137, 321 (1993)
doi:10.1002/pssa.2211370205
[51] V.V. Kveder, A.E. Koshelev, T.R. Mchedlidze, Yu.A. Osipian, A.I. Shalynin, Sov. Phys. JETP 68(1), 104 (1989)
doi:10.4028/www.scientific.net/SSP.6-7.301
[52] M. Wattenbach, C. Kisielowski-Kemmerich, H. Alexander, V.V. Kveder, T.R. Mchedlidze, Yu.A. Osipian, Phys. Stat. Sol. (b), 158, K49 (1990)
doi:10.1002/pssb.2221580150
[53] V.V. Kveder, Solid State Phenomena 32-33, 279 (1993)
doi:10.4028/www.scientific.net/SSP.32-33.279
[54] V. Kveder, T. Sekiguchi, K. Sumino, Phys.Rev. B 51(23), 16721 (1995)
doi:10.1103/PhysRevB.51.16721
[56] V.V. Kveder, A.I. Shalynin, E.A. Steinman, A.N. Izotov, Solid State Phenomena 57-58, 299 (1997)
doi:10.4028/www.scientific.net/SSP.57-58.299
[57] G. Dresselhaus, Phys. Rev. 100, 580 (1955)
doi:10.1103/PhysRev.100.580
[61] M. Kittler, M.Reiche, W. Seifert, X. Yu, T. Arguirov, O.F. Vyvenko, T. Mchedlidze, T. Wilhelm, ECS Transactions 3(4), 429 (2006)
doi:10.1149/1.2355777

[62] X. Yu, T. Arguirov, M. Kittler, W. Seifert, M. Ratzke, M. Reiche, Mater. Sci. Semicond. Processing 9, 96 (2006)
doi:10.1016/j.mssp.2006.01.070
[63] M. Kittler, M. Reiche, T. Arguirov, T. Mchedlidze, W. Seifert, O.F. Vyvenko, T. Wilhelm, X. Yu, Solid State Phenomena Vols. 131-133, 289 (2008)
doi:10.4028/www.scientific.net/SSP.131-133.289
[67] M. Kittler, C. Ulhaq-Bouillet, V. Higgs, J. Appl. Phys. 78, 4573 (1995)
doi:10.1063/1.359802
[68] M. Kittler, W. Seifert, Scanning Microscopy 15, 316 (1993)
doi:10.1002/pssa.2211370206
[69] M. Kittler, W. Seifert, V. Higgs, Phys. Stat. Sol. (a) 137, 327 (1993)
doi:10.1002/pssa.2211370206
[70] K. Knobloch, M. Kittler, W. Seifert, J.J. Simon, I. Perichaud, Solid State Phenomena 63-64, 105 (1998)
doi:10.4028/www.scientific.net/SSP.63-64.105
[71] S. Kusanagi, T. Sekiguchi, B. Shen, K. Sumino, Mater. Sci. Technology 11, 685 (1995)
doi:10.4028/www.scientific.net/MSF.196-201.1195
[74] N. A. Drozdov, A. A. Patrin, V. D. Tkachev, Phys. Stat. Sol. (b) 83, K137 (1977)
doi:10.1002/pssb.2220830245
[75] R. Sauer, J. Weber, J. Stolz, E.R. Weber, K.-H. Küsters, H. Alexander, Appl. Phys. A 36, 1 (1985)
doi:10.1007/BF00616453
[76] J. Weber, Solid State Phenomena 37-38, 13 (1994)
doi:10.4028/www.scientific.net/SSP.37-38.13
[77] K. Weronek, PhD Thesis Stuttgart, Germany 1992
doi:10.4028/www.scientific.net/MSF.83-87.1315
[80] R. Sauer, Ch. Kisielowski-Kemmerich, H. Alexander, Phys. Rev. Lett. 57, 1472 (1986)
doi:10.4028/www.scientific.net/MSF.10-12.745
[81] K. Wessel, H. Alexander, Phil. Mag. 35, 1523 (1977)
doi:10.1080/14786437708232975
[82] H. Alexander, H. Eppenstein, H. Gottschalk, S. Wendler, J. Microsc. 118, 13 (1980)
doi:10.1119/1.2340630
[83] V. Higgs, E.C. Lightowlers, E.A. Fitzgerald, Y.-H. Xie, J. Silverman, J. Appl. Phys. 73, 1952 (1993)
doi:10.1063/1.353185
[84] G.P. Watson, J.L. Benton, Y.H. Xie, E.A. Fitzgerald, J. Appl. Phys. 83, 3773 (1998).
doi:10.1063/1.366606
[85] R. Jones, B.J. Coomer, J.P. Goss, S. Öberg, P.R. Briddon, Phys. Stat. Sol. (b) 222, 133 (2000)
doi:10.1002/1521-3951(200011)222:1<133::AID-PSSB133>3.0.CO;2-D
[89] M. Kittler, M. Reiche, X. Yu, T. Arguirov, O.F. Vyvenko, W. Seifert, T. Mchedlidze, G. Jia, T. Wilhelm, Tech. Digest IEDM 2006, pp. 845-848
doi:10.1109/IEDM.2006.346912
[90] M. Kittler, M. Reiche, W. Seifert, X. Yu, T. Arguirov, O.F. Vyvenko, T. Mchedlidze, T. Wilhelm, ECS Transactions 3(4), 429 (2006)
doi:10.1149/1.2355777
[91] M. Kittler, M. Reiche, T. Mchedlidze et al., 'Photonics West' to be held in San Jose, Jan. 2008, Proc. SPIE "Silicon Photonics III", manuscript # 6898-12

doi:10.1117/12.773295
[92] T. Mchedlidze, T. Arguirov, M. Kittler, T. Hoang, J. Holleman, J. Schmitz, Appl. Phys. Lett. 91, 201113 (2007)
doi:10.1063/1.2813024
[93] D.A.B. Miller, D.S. Chemla, T.C. Damen, A.C. Gossard, W. Wiegmann, T.H. Wood, C.A. Burrus, Phys. Rev. B 32, 1043 (1985)
doi:10.1049/el:19850490
[3] M. Oehme, J. Werner, M. Jutzi, G. Whl, E. Kasper, M. Berroth, Thin Solid Films 508, 393 (2006)
doi:10.1016/j.tsf.2005.06.106
[7] J. Chevrier, J.Y. Natoli, I. Berbezier, A. Ronde, J. Derrien, Solid State Phenomena Vols. 3233, 39 (1993)
doi:10.4028/www.scientific.net/SSP.32-33.39
[12] V. Kveder, M. Badylevich, E. Steinman, A. Izotov, M. Seibt, W. Schrter, Appl. Phys. Lett. 84, 2106 (2004)
doi:10.1063/1.1689402
[13] V. Kveder, M. Badylevich, W. Schrter, M. Seibt, E. Steinman, A. Izotov, Phys. Stat. Sol. (a) 202, 901 (2005)
doi:10.1002/pssa.200460512
[17] R. Sauer, J. Weber, J. Stolz, E.R. Weber, K.-H. K□sters, H. Alexander, Appl.Phys. A 36, 1 (1985)
doi:10.1007/BF00616453
[31] V.V. Kveder, Yu.A. Osipian, W. Schrter, G. Zoth, Phys.Stat. Sol. (a), 72,701-713, (1982)
doi:10.1002/pssa.2210720233
[37] W. Schrter, V. Kveder, H. Hedemann, Solid State Phenomena 82-84, 213 (2002)
doi:10.4028/www.scientific.net/SSP.82-84.361
[38] V. Kveder, W. Schrter, M. Seibt, A. Sattler, Solid State Phenomena 82-84, 361 (2002)
doi:10.4028/www.scientific.net/SSP.82-84.361
[65] V. Kveder, M. Kittler, W. Schrter, Phys. Rev. B 63, 115208 (2001)
doi:10.1103/PhysRevB.63.115208
[91] M. Kittler, M. Reiche, T. Mchedlidze et al., `Photonics West' to be held in San Jose, Jan. 2008, Proc. SPIE "Silicon Photonics III", manuscript # 6898-12
doi:10.1117/12.773295